Chem Soc Rev

Energy Transfer in Lanthanide Upconverting Studies for Extended Optical Applications

SCHOLARONE™
Manuscripts

Journal Name

ARTICLE

Energy Transfer in Lanthanide Upconverting Studies for Extended Optical Applications

Hao Dong, Ling-Dong Sun*, and Chun-Hua Yan*

Lanthanide pairs, which can upconvert low energy photons into higher ones, is promising for efficient upconversion emission. A typical system with Yb^{3+} as sensitizer, could convert short NIR into visible/ultraviolet light *via* energy transfer between lanthanide ions. These upconversion nanocrystals doped with lanthanide ions have found significant potentials in bioimaging, photochemical reactions and energy conversion. This review presents a fundamental understanding of energy transfer in lanthanides supported photon upconversion. We introduce the emerging progresses in excitation selection based on the energy transfer within lanthanide ions or activated from antennas, with an outlook in development and applications of the lanthanide upconversion emissions.

1. Introduction

Benefiting from abundant energy levels of 4f configurations, trivalent lanthanide ions (Ln^{3+}) are endowed with unique and fascinating optical properties. Possessing the real intermediate energy levels, Ln^{3+} could give out desired emissions *via* various energy transfer pathways. Inheriting their native intra-configurational transitions, Ln^{3+} activated luminescent materials has been receiving consistent attraction due to their excellent photostability and long luminescence lifetime, as well as the large Stokes/anti-Stokes shifts and sharp-band emissions.[1–3] As a consequence, Ln^{3+} based luminescent materials have found a wide range of applications, such as lighting and displays, biomarkers, drug carriers, and photovoltaic devices.[4–10]

Part of the energy levels of Ln^{3+}, which embody Ln^{3+} contained luminescence materials with various energy transfer potentials, are depicted in Fig. 1a. Three typical energy transfer modes of Ln^{3+} are shown in Fig. 1b, namely downshifting (DS), quantum cutting (QC) and upconversion (UC) emissions. Unlike the former two cases, UC is a non-linear optical process which requires two or more low energy near infrared (NIR) photons to generate a higher one, ranging from NIR to visible and even ultraviolet (UV) region, which was firstly proposed by N. Bloembergen in 1959.[12] Since then, numerous efforts were made to enrich the family of UC luminescent materials, and Ln^{3+} based bulk materials have been successfully devoted to display devices and compact solid state lasers.[1] With the development of nanotechnologies, UC luminescent materials have been developed into nanoscale for more prospects, and types of upconversion nanoparticles (UCNPs) of various size and composition have been prepared.[13–21]

Ln^{3+} doped UCNPs are of great interest in many aspects. Emissions from conventionally used quantum dots and organic dyes are sensitive to the size and chemical surroundings.[3] In contrast, UC emissions resulting from 4f–4f intra-configurational transitions are shielded by neighboring $5s^25p^6$ shells, and this is responsible for the emissions that are independent on the particle size and environments.[22,23] Fixed energy levels, high resistance to photoblinking and photobleaching, micro/milli-second lifetime, and large anti-Stokes shifts are also typical optical features for UCNPs. Moreover, when it comes to biological purposes, UCNPs are superior in the unique NIR triggered anti-Stokes emissions. UCNPs offer minimized photodamage, high signal-to-noise ratio and remarkable penetration depth for *in vitro* and *in vivo* applications, *etc*.[3,24-26]

The advantage of Ln^{3+} doped UCNPs could also be attributed to their highly efficient conversion of NIR photons to visible/UV photons. A continuous-wavelength (CW) laser can be used to induce Ln^{3+} supported UC emissions ($1 - 10^3$ W cm^2). On the contrary, simultaneous two-photon absorption (TPA) process requires femtosecond pulsed laser excitation in quantum dots and organic dyes ($10^6 - 10^9$ W cm^2), which are without intermediate energy levels.[14]

Featured with abundant fixed energy levels, Ln^{3+} supported UC emissions proceed *via* various mechanisms. The color of such emissions may vary with different energy transfer pathways.[22] It is worth mentioning that intrinsic energy transfers in Ln^{3+} doped UCNPs play a dominant role in determining the UC emission efficiency. Consequently, it is essential to rationally modify the energy transfer routes in order to obtain satisfactory UC emission efficiency and desired color outputs. In addition, the demand of specific UC emissions highlights the importance of energy transfer studies.

This review focuses mainly on the energy transfer routes in Ln^{3+} doped UCNPs upon NIR irradiation. Herein, we (i) present a fundamental understanding of Ln^{3+} related UC emissions; (ii) describe the mainstream energy transfer related UC emission modulation methods; (iii) additionally introduce the progresses in broadening the excitation for photon upconverting process, typical results from organic antenna or energy transfer in lanthanide.

2. Mechanisms of UC emissions

The abundant energy levels of Ln^{3+} endow them with various energy transfer pathways for UC emissions. In general, UC mechanisms are categorized into five classes: (*a*) excited states absorption (ESA, Fig. 2a); (*b*) energy transfer upconversion (ETU, Fig. 2b); (*c*) photon avalanche (PA, Fig. 2c); (*d*) cooperative energy transfer (CET, Fig. 2d), and (*e*) energy migration-mediated upconversion (EMU, Fig. 2e).[1] It is worth noting that different energy transfer processes result in distinctive UC efficiency, and that there is no universal mechanism for any of the luminescent Ln^{3+}.

An ESA process refers to a sequential absorption of two
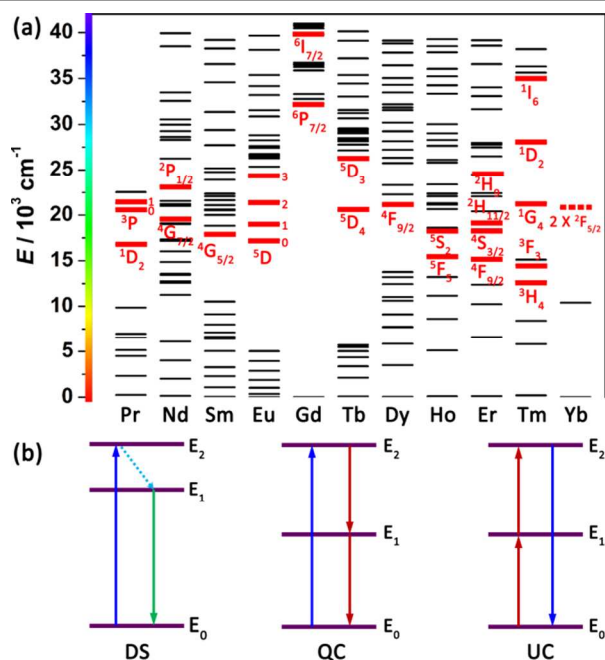
Fig. 1 (a) Partial energy level diagrams of Ln^{3+}. Corresponding typical UC emissive excited levels are highlighted with red bold lines. (b) Schematic illustrating for three energy transfer modes of Ln^{3+}. From left to right are downshifting (DS), quantum cutting (QC), and upconversion (UC). Upward and downward full arrows stand for photon excitation and emission processes, respectively. Dashed line represents non-irradiative relaxation process.

pump photons by a single ion which is possessed of multiple energy levels. Therefore, intermediate energy level of luminescent centers should be stable with adequate electron populations. This promises the sequential absorption of a second pump photon. High pump power density and large absorption cross-section facilitate ESA processes. These rigorous requirements hinder the generalization of ESA processes. Furthermore, ESA process is more likely to occur with a low doping concentration (<1%), for high doping concentration could lead to prominent non-radiative cross-relaxations to deteriorate the emission intensity significantly.

Unlike ESA, ETU is much more efficient. Two different types of ions, namely sensitizer and activator, are embedded in the upconverting unit, where the absorption cross-section of sensitizer is larger than that of activator. Upon excitation of lower energy photons, both sensitizer and activator could be pumped to their excited states. Subsequently, the sensitizer donates the energy to activator non-radiatively *via* dipole-dipole resonant interaction. Ln^{3+} ions with multiple excited states show great advantage for ETU process.

PA was firstly proposed by Chivian *et al.* in a Pr^{3+} based infrared quantum counter in 1979.[27] As shown in Fig. 2c, the energy gap between the intermediate and ground state of the luminescent centers does not match with the energy of the pump photon. In this case, luminescent centers may undergo an ESA process to populate higher excited state (superexcited) if certain electrons are promoted to the intermediate state. Then cross-relaxation resonantly occur between the superexcited ions and a neighboring ground state ions, leading to the occupation of intermediate states of both two ions. The repeating of such process populates the intermediate states exponentially above the excitation threshold. In such ways, avalanche transitions readily occur as long as the consumption of superexcited ions is less than that of ground state ones. PA related UC emissions are much less efficient, especially in nanomaterials. To date, there is only one report of PA based UC emissions in $LnVO_4$ nanocrystals (NCs, Ln = Ce, Nd).[28]

Similar to ETU, both sensitizers and activators are important for a CET based UC process. The main difference is that there is no real intermediate energy level in the activator. In a typical CET process, two sensitizers cooperatively activated to a virtual excited state to fulfill a simultaneously energy transfer to a neighboring activator.[29] Except for the UC emission from activators, cooperative UC emissions from sensitizers could also be observed with low efficiency.[1] CET related studies have been mainly focused on bulk materials, as well as polymers and glasses.[29–31] Only few published works proved the feasibility of CET based UC emissions in nanomaterials.[32,33]

To further enhance the efficiency of UC emissions from activators that without proper intermediate energy levels, Liu and coworkers proposed a novel energy transfer pathway, namely energy migration-mediated upconversion (EMU).[34] In a

typical EMU process, four types of luminescent centers are incorporated into separated layers with precisely defined
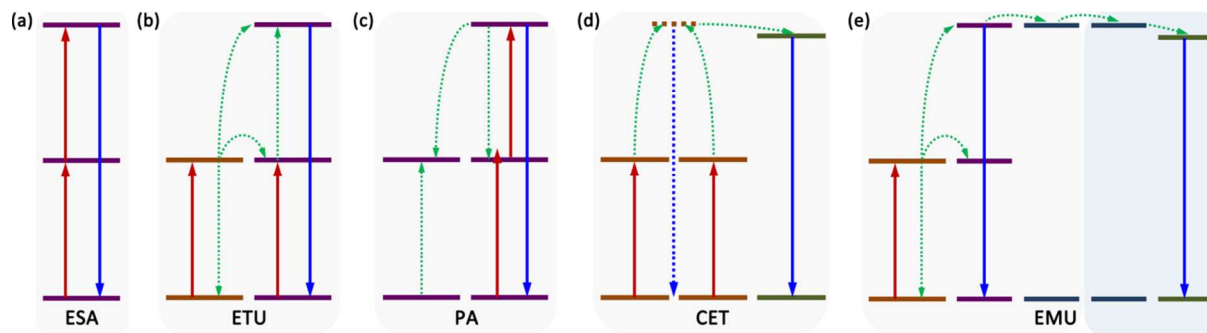
Fig. 2 Schematic representation of UC processes, where upward (red) and downward (blue) full arrows stand for direct excitation processes and radiative emission processes, respectively. Dashed arrows (green) represent energy transfer processes. Note that non-radiative relaxations are not given here for clarity. Different kind of luminescent centers are shown with different colored energy levels, and different regions are highlighted with different background colors. (a) ESA, (b) ETU, (c) PA, (d) CET, (e) EMU.

process occurs *via* the following steps: (i) the population of the higher excited state of accumulator *via* an ETU process; (ii) the absorbed energy migrates from the high-lying excited state of accumulator to migrator, followed by further energy transfer through the core/shell interface within migrator ions; (iii) the energy is trapped by neighboring activator. Radiative emissions from activator and accumulator are observed as electrons return to the ground states.

As mentioned above, the UC efficiency varies when adopting different energy transfer pathways. The efficiency of ESA is limited by pump power density and absorption cross-section of Ln^{3+}. PA is a special UC energy transfer manner which closely relies on cross-relaxation within luminescent centers and excitation power density. As a result, PA shows a delayed response to pumps due to certain required cycles of cross-relaxations and ESA processes. Usually, PA occurs in systems with high doping concentration under excitation of high power density, which offers high probability of cross-relaxations. The rigorous conditions limit PA for extensive applications except for compact lasers. When it comes to CET process, high doping ratio of cooperative sensitizers is required to meet sufficient sensitization. Nevertheless, UC efficiency of CET is rather low due to the lack of real intermediate states, which is also illustrated in nanomaterials. Of all the five energy transfer mechanisms for UC emissions, ETU is considered the most efficient. In the past decades, Auzel, and Cases *et al.* have made pioneering and outstanding contributions to the measurements of efficiency of the energy transfer pathways. In their studies, the quantum efficiency of the ETU process was *ca*. 10^{-3}, while that of the ESA and CET process was *ca*. 10^{-5} and 10^{-6}, respectively.[35–39] To date, ETU based UCNPs have been overwhelmingly dominating in relative studies. To some extent, EMU is an extension of ETU benefits from lanthanide ions with distinctive energy levels introduced into separated layers.

3. Composition of UCNPs

concentrations. The four kinds of luminescent centers are sensitizer, accumulator, migrator and activator. An EMU

An emissive UCNP is composed of an optical inert host matrix and optical active Ln^{3+} as luminescent centers. Luminescent Ln^{3+} ions are embedded in the matrix with replacing cations of the matrix during the NC formation. It is worth mentioning that UC emissions rely heavily on the composition of NCs. Theoretically, UCNPs should give out desired emission so long as the selected luminescent centers are doped into a certain host lattice.

3.1 Host Matrix

Different host matrix has different coordination number, energy transfer distance between luminescent centers, and efficiency of energy transfer. Thus it is of great importance to screen the host matrix. An ideal host matrix should be equipped with four properties: (*a*) high tolerance for luminescent centers; (*b*) low phonon energy to minimize deleterious non-radiative relaxations; (*c*) high transparency for free migration of NIR photons in the lattice; (*d*) excellent chemical and thermostability to keep original crystal structures.

Because of the similar valence state, chemical and physical properties, trivalent optical inert rare earth ions (RE^{3+}, RE = Ln Sc, and Y) based inorganic compounds are usually employed as the host matrix. To date, RE based oxides,[40] oxysulfides,[41] oxysalts[42] and fluorides[43] have been investigated. Apart from these, some other alkaline earth ions and transition metal ions based compounds are also used as host materials. For example, Ca^{2+}, Zr^{4+}, *et al.*[44,45] Among the reported host materials, $NaREF_4$ series have been proved optimum due to their relative low phonon energy and excellent chemical stability.[46,47] There are two phase structures of $NaREF_4$ NCs, namely cubic phase (α) and hexagonal phase (β). It is generally adopted that β-$NaREF_4$ families are more efficient due to their unique crystal structure.[48] Hence, β-$NaREF_4$ series have been chosen as most common nanosized host lattices for decades. As for bulk materials, oxides and fluoride based glasses are most frequently employed as efficient upconverting supporters.

3.2 Sensitizer

According to ETU process, the ideal sensitizers should possess relatively large absorption cross-section and energy levels matching with those of activators, while the excited energy state locates at NIR region. Among all the Ln^{3+} shown in Fig. 1a, Yb^{3+} is the best choice. Absorption cross-section of Yb^{3+} is 9.11×10^{-21} cm^{-2} (976 nm, $^2F_{7/2} \rightarrow {}^2F_{5/2}$), relatively large among Ln^{3+} ions. Most importantly, the energy level diagram of Yb^{3+} is quite simple, with only one excited state of $^2F_{5/2}$. From Fig. 1a, we can also find that the energy of excited states of Yb^{3+} is similar to that of Er^{3+}, Tm^{3+} *etc*. These make Yb^{3+} an excellent sensitizer to donate energy to others.

3.3. Activator

For ETU process, activators should possess adequate long-lived intermediate energy states. Once electrons of the ground state are excited to intermediate one, activators are likely to extract energy from nearby excited sensitizers to promote further transition to higher energy levels. On the other hand, energy levels of activators should not be close. Otherwise, detrimental non-radiative relaxations, whose rate decreases exponentially with increasing energy gap, would dominate. Based on these considerations, Er^{3+}, Tm^{3+} and Ho^{3+} (especially Er^{3+} and Tm^{3+}) are ideal ETU activators because of ladder-like arranged energy levels.[14,22] Among the three commonly used ETU activators, Er^{3+} shows the highest UC efficiency. This should be attributed to the similar energy gap from $^4I_{15/2}$ to $^4I_{11/2}$ (first upward transition) and $^4I_{11/2}$ to $^4F_{7/2}$ (second upward transition).

Actually, Ln^{3+}, except La^{3+} ($4f^0$), Ce^{3+} ($4f^1$) and Lu^{3+} ($4f^{14}$), could produce diverse efficient UC emissions through proper energy transfer processes as well, even Yb^{3+} ions. Nd^{3+} doped UCNPs can generate UC emissions *via* ESA process.[49,50] With ETU processes, $Yb^{3+} - Pr^{3+}$,[51,52] $Yb^{3+} - Sm^{3+}$,[53] and $Yb^{3+} - Dy^{3+}$ pairs[54,55] can generate UC emissions in a great extent. However, the UC emission efficiency is rather low due to prominent non-radiative relaxations within activators.

Due to the absence of long-lived intermediated energy levels, Eu^{3+} and Tb^{3+} cannot capture necessary energy to complete two upward transitions. Thus, ETU is not applicable to get the UC emissions. However, UC emissions could also be observed with $Yb^{3+} - Eu^{3+}/Yb^{3+} - Tb^{3+}$ pairs, whose mechanism was proved

to be CET process.[56] Despite no ladder-like low energy excited states, purely Yb^{3+} doped NCs could also generate blue cooperative UC emissions due to formation of $Yb^{3+} - Yb^{3+}$ dimers.[57]

Another special case is Gd^{3+}. Obviously, the first excited state of Gd^{3+} (~ 32224 cm^{-1}) is much higher than that of other Ln^{3+}. Therefore, energy transfer to Gd^{3+} could not be happened directly even from dimers of Yb^{3+} (CET). The reported UC emissions *via* Gd^{3+} are derived from energy transfer from high-lying excited state of Tm^{3+}.[58] Typical UC emissions with their corresponding transitions of each Ln^{3+} are listed in Table 1.

4. Energy Transfer in $Yb^{3+} - Er^{3+}$, $Yb^{3+} - Tm^3$ pairs

As mentioned above, ETU process activated with Er^{3+} and Tm^{3+} are optimized for UC emission studies. The doping content of Yb^{3+} is usually kept at 20% or higher, while that of the activator normally lower than 2%. Such large content difference is attributed to the intrinsic character of f-configurations. As the energy levels of the activators are generally complicated and dense, low doping ratio minimizes undesirable multiphoton cross-relaxations. On the contrary, the energy level scheme of Yb^{3+} is quite simple, and thus shows certain tolerance to high doping concentration, which can greatly increase the absorption probability of NIR photons. However, there usually an optimal doping concentration, more Yb^{3+} would result in cross-relaxations between $Yb^{3+} - Yb^{3+}$ pairs.

Upon 980 nm irradiation, UC emissions from Er^{3+} and Tm^{3+} could range from NIR region to visible and UV region (Fig. 3). In order to understand the UC emission processes in details, the UC energy transfer processes in most frequently used $Yb^{3+} - Er^{3+}$ and $Yb^{3+} - Tm^{3+}$ pairs are discussed. An important parameter, the number of photons involved in the UC process, should be well characterized. This can be obtained from the slope of log-log diagram of UC luminescence intensity *versus* the pumping power, which is often recorded as *I–P* curve. Güdel and coworkers for the first time proposed the theoretical dependence.[63] Furthermore, they verified the theoretical results

Table 1 Typical lanthanide activators and corresponding UC emissions and transitions

Activators	UC emissions (nm)	Corresponding transitions	Ref.
Pr^{3+}	485, 520, 538, 605, 635, 645, 670, 690, 720	$^3P_0 \rightarrow {}^3H_4$, $^3P_1 \rightarrow {}^3H_5$, $^3P_0 \rightarrow {}^3H_5$, $^1D_2 \rightarrow {}^3H_4$, $^3P_0 \rightarrow {}^3F_2$, $^3P_0 \rightarrow {}^3H_6$, $^3P_1 \rightarrow {}^3F_3$, $^3P_0 \rightarrow {}^3F_3$, $^3P0 \rightarrow {}^3F_4$	51, 52
Nd^{3+}	430, 482, 525, 535, 580, 600, 664, 766	$^2P_{1/2} \rightarrow {}^4I_{9/2}$, $^2P_{1/2} \rightarrow {}^4I_{11/2}$, $^2P_{1/2} \rightarrow {}^4I_{13/2}$, $^4G_{7/2} \rightarrow {}^4I_{9/2}$, $^2P_{1/2} \rightarrow {}^4I_{15/2}$, $^4G_{7/2} \rightarrow {}^4I_{11/2}$ and $^4G_{5/2} + {}^2G_{7/2} \rightarrow {}^4I_{9/2}$, $^4G_{7/2} \rightarrow {}^4I_{13/2}$, $^4G_{7/2} \rightarrow {}^4I_{15/2}$	49, 50
Sm^{3+}	520, 541, 555, 590, 646, 657, 700, 799 – 873	$^4G_{7/2} \rightarrow {}^6H_{5/2}$, $^4F_{3/2} \rightarrow {}^6H_{5/2}$, $^4G_{5/2} \rightarrow {}^6H_{5/2}$, $^4G_{5/2} \rightarrow {}^6H_{7/2}$, $^4G_{7/2} \rightarrow {}^6H_{9/2}$, $^4G_{7/2} \rightarrow {}^6H_{11/2}$, $^6F_{11/2} \rightarrow {}^6H_{5/2}$	53, 34
Eu^{3+}	416, 429, 490, 510, 535, 554, 590, 613	$^5D_3 \rightarrow {}^7F_1$, $^5D_3 \rightarrow {}^7F_2$, $^5D_2 \rightarrow {}^7F_2$, $^5D_2 \rightarrow {}^7F_3$, $^5D_1 \rightarrow {}^7F_1$, $^5D_1 \rightarrow {}^7F_2$, $^5D_0 \rightarrow {}^7F_1$, $^5D_0 \rightarrow {}^7F_2$	51, 34
Gd^{3+}	278, 305, 312	$^6I_{7/2} \rightarrow {}^8S_{7/2}$, $^6P_{5/2} \rightarrow {}^8S_{7/2}$, $^6P_{7/2} \rightarrow {}^8S_{7/2}$	58
Tb^{3+}	381, 415, 438, 489, 541, 584, 619	$^5D_3 \rightarrow {}^7F_6$, $^5D_3 \rightarrow {}^7F_5$, $^5D_3 \rightarrow {}^7F_4$, $^5D_4 \rightarrow {}^7F_6$, $^5D_4 \rightarrow {}^7F_5$, $^5D_4 \rightarrow {}^7F_4$, $^5D_4 \rightarrow {}^7F_3$	33, 34, 56
Dy^{3+}	378, 408, 487, 543, 569, 570, 610, 655, 663	$^4G_{11/2} \rightarrow {}^6H_{13/2}$, $^4G_{9/2} \rightarrow {}^6H_{13/2}$, $^4G_{9/2} \rightarrow {}^6H_{11/2}$, $^4I_{15/2} \rightarrow {}^6H_{13/2}$, $^4G_{11/2} \rightarrow {}^6H_{111/2}$, $^4F_{9/2} \rightarrow {}^6H_{13/2}$, $^4G_{11/2} \rightarrow {}^6H_{9/2}$, $^4G_{11/2} \rightarrow {}^6H_{7/2}$, $^4F_{9/2} \rightarrow {}^6H_{11/2}$	34, 54, 55
Ho^{3+}	542, 655	$^5F_4, {}^5S_2 \rightarrow {}^5I_8$, $^5F_5 \rightarrow {}^5I_8$	59, 60
Er^{3+}	415, 525, 542, 655	$^2H_{9/2} \rightarrow {}^4I_{15/2}$, $^2H_{11/2} \rightarrow {}^4I_{15/2}$, $^4S_{3/2} \rightarrow {}^4I_{15/2}$, $^4F_{9/2} \rightarrow {}^4I_{15/2}$	61
Tm^{3+}	290, 345, 362, 450, 475, 644, 694, 800	$^1I_6 \rightarrow {}^3H_6$, $^1I_6 \rightarrow {}^3F_4$, $^1D_2 \rightarrow {}^3H_6$, $^1D_2 \rightarrow {}^3F_4$, $^1G_4 \rightarrow {}^3H_6$, $^1G_4 \rightarrow {}^3F_4$, $^3F_3 \rightarrow {}^3H_6$, $^3H_4 \rightarrow {}^3H_6$	58, 62
Yb^{3+}	450 – 500	$2 \times {}^2F_{5/2} \rightarrow {}^2F_{7/2}$ (Cooperative Emission)	57
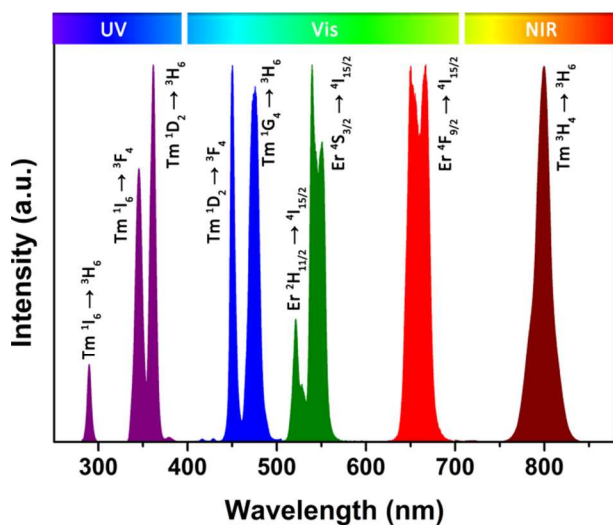
Fig. 3 Typical UC emissions, ranging from UV to NIR regions, from Yb^{3+} – Er^{3+} and Yb^{3+} – Tm^{3+} co-doped UCNPs under 980 nm excitation. All the emissions are normalized to the emission intensity of each region.

in Ln^{3+} and transition-metal-ion systems.[64] In practical investigations, the number of photons involved in the corresponding UC process could be obtained from slope of the I–P curves.

4.1 Yb^{3+} – Er^{3+} Pairs

In Yb^{3+} – Er^{3+} co-doped UCNPs, green emissions (525 nm and 542 nm) and red emissions (655 nm) are mostly observed under 980 nm excitation, while emission at 415 nm can also be given. We systematically studied UC properties from Yb^{3+} – Er^{3+} co-doped $NaYF_4$ NCs.[61] Typical I–P curves showed that green emissions and red emission were both generated from two-photon processes, while the violet emission from a three-photon process. These UC mechanisms are shown in Fig. 4a, where the superb resonance between the $^2F_{7/2} \rightarrow {}^2F_{5/2}$ transition of Yb^{3+} and the $^4I_{15/2} \rightarrow {}^5I_{11/2}$ transition of Er^{3+} is clearly illustrated.

This good level-matching offers efficient energy transfer from Yb^{3+} to Er^{3+}.

Upon 980 nm CW laser irradiation, Yb^{3+} absorbs the NIR photons with the generating of $^2F_{7/2} \rightarrow {}^2F_{5/2}$ upward transitions. Subsequently, it donates the energy to the adjacent Er^{3+} resonantly with Yb^{3+} dropping back to its $^2F_{7/2}$ ground state. This promotes Er^{3+} ions getting to the excited states (route 1, $^4I_{15/2} \rightarrow {}^4I_{11/2}$). Due to the energy level match, the Er^{3+} ions could be populated to its higher excited state via similar resonant energy from sensitizers (route 2, $^4I_{11/2} \rightarrow {}^4F_{7/2}$ or $^4I_{13/2} \rightarrow {}^4F_{9/2}$). The super-excited Er^{3+} relax to $^2H_{11/2}$ and $^4S_{3/2}$ states non-radiatively. As electrons return to the ground states, green emissions corresponding to 525 and 542 nm, respectively, could give out. Alternatively, electrons from the $^4F_{9/2}$ state, non-radiatively populated from higher energy levels or resonant energy transfer from $^4I_{13/2}$, resulting in red emissions centered at 655 nm via $^4F_{9/2} \rightarrow {}^4I_{15/2}$ transition. Therefore, green and red emissions can be simultaneously obtained through two-photon UC processes.

The weak violet emission at 415 nm is attributed to a three-photon process. The proposed energy transfer processes are also shown in Fig. 4a. $^4F_{9/2}$ state of Er^{3+} has the probability to accept another NIR photon from Yb^{3+} to arrive at much higher excited states (route 3, $^4F_{9/2} \rightarrow {}^4G_{11/2}$). With the relaxation to $^2H_{9/2}$ state, transitions of $^2H_{9/2} \rightarrow {}^4I_{15/2}$ release violet photons.

Moreover, we also discovered the interesting green ($^4S_{3/2} \rightarrow {}^4I_{15/2}$) and red ($^4F_{9/2} \rightarrow {}^4I_{15/2}$) emissions from three photon processes in small sized β-$NaYF_4$:Yb,Er NCs at high pumping power density. For the green emission, it is suggested that electrons on the $^4F_{7/2}$ state can be further promoted to $^4G_{11/2}$ state by an ETU process from Yb^{3+} followed by two cross-relaxation processes: $^4I_{15/2}$ (Er^{3+}) + $^4G_{11/2}$ (Er^{3+}) $\rightarrow {}^4I_{13/2}$ (Er^{3+}) + $^2H_{11/2}$ (Er^{3+}) or $^4S_{3/2}$ (Er^{3+}), and $^4I_{9/2}$ (Er^{3+}) + $^4G_{11/2}$ (Er^{3+}) $\rightarrow {}^2H_{11/2}$ (Er^{3+}) + $^2H_{11/2}$ (Er^{3+}) or $^4S_{3/2}$ (Er^{3+}). For the $^4F_{9/2} \rightarrow {}^4I_{15/2}$ transition, after electrons populated the $^4S_{3/2}$ state via a two-photon process, the following cross-relaxation between Er^{3+} ions occurs: $^4I_{15/2}$ (Er^{3+}) + $^4S_{3/2}$ (Er^{3+}) $\rightarrow {}^4I_{13/2}$ (Er^{3+}) + $^4I_{9/2}$

(Er^{3+}). This implies the population of $^4I_{13/2}$ state is a two-photon UC process. After the cross-relaxation, $^4F_{9/2}$ state is populated. The green and red emissions exhibit three-photon UC properties because of these cross-relaxations.

4.2 Yb^{3+} – Tm^{3+} Pairs

As for Yb^{3+} – Tm^{3+} doped UCNPs, the 290/345/362 nm UV emissions, the 450/475/644/694 nm visible emissions, as well as the 800 nm NIR emission can all be given under 980 nm irradiation simultaneously. We have comprehensively investigated the UC characters of β-NaYF₄:Yb,Tm NCs.[62] *I–P* curves monitored by varying excitation power density indicated that the emissions at 290 and 345 nm result from five-photon processes, and emissions at 362 and 450 nm, 475 and 644 nm, 694 nm and 800 nm come from four-photon, three-photon and two-photon processes respectively.

Compared with Yb^{3+} – Er^{3+} pairs, the UC emission from Yb^{3+} – Tm^{3+} pairs may involve more than two photons. This is ascribed to the discrete and ladder-like arranged energy levels from Tm^{3+}. In contrast, the dense energy levels of Er^{3+} at high wave-number domain cause considerable deleterious non-radiative relations, and thus greatly reduce the probability of multi-photon upward transitions.

Similar to the case of Yb^{3+} – Er^{3+} pairs, Yb^{3+} ions also play the role of absorbing 980 nm photons in Yb^{3+} – Tm^{3+} pairs. As the excited electrons relax to the ground state (Yb^{3+}, $^4F_{7/2}$), an energy migration occur to the $^3H_5$ state of a neighbouring Tm^{3+} non-radiatively (Fig. 4, route 1, $^3H_6 \rightarrow {}^3H_5$). Then, electrons relaxed to the $^3F_4$ states, giving the $^3F_4 \rightarrow {}^3F_2$ upward transition *via* resonant energy from Yb^{3+} (route 2). Then the $^3F_3$ and $^3H_4$ state are populated through a relaxation process, followed by $^3F_3 \rightarrow {}^3H_6$ (694 nm) and $^3H_4 \rightarrow {}^3H_6$ (800 nm) transitions. In most cases, the two-photon emissions dominate the UV – NIR spectral regime due to its relative high efficiency.

With high pump power density, the active electrons on the $^3H_4$ state can be further excited *via* $^3H_4 \rightarrow {}^1G_4$ (route 3), $^1G_4 \rightarrow {}^1D_2$ (route 4), and $^1D_2 \rightarrow {}^3P_2$ (route 5) upward transitions. Electrons at the $^3P_2$ state relax non-radiatively to populate the
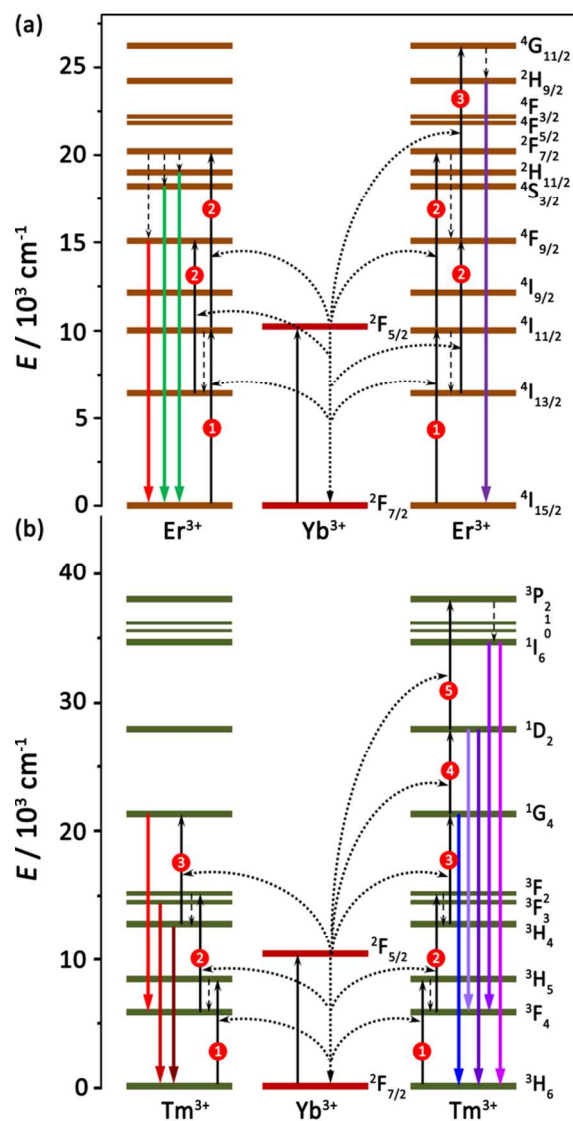
Fig. 4 Proposed energy transfer mechanisms illustrating UC energy transfer processes in Yb^{3+} – Er^{3+} and Yb^{3+} – Tm^{3+} co-doped UCNPs under 980 nm irradiations. (a) UC energy transfer in Yb^{3+} – Er^{3+} pairs. On the left are two-photon UC processes, generating red and green emissions. On the right is three-photon UC process, yielding violet emissions. (b) UC energy transfer processes in Yb^{3+} – Tm^{3+} pairs. Left half diagram represents two- and three-photon UC processes, producing NIR and visible radiative emissions. Right half diagram stands for three-, four-, and five-photon UC processes. Short wavelength visible and UV emissions are given out through these multi-photon UC transitions. Note that black full arrows are upward UC transitions, dotted arrows and dashed arrows are energy transfer and relaxation processes, respectively. Colored downward full arrows represent radiative UC emissions. Numbers in red circles represent the number of photons involved in population on corresponding excited states.

$^1I_6$ state. From these three high-lying states, the following electron transitions occur and result in radiative transitions of $^1G_4 \rightarrow {}^3F_4$ (644 nm), $^1G_4 \rightarrow {}^3H_6$ (475 nm), $^1D_2 \rightarrow {}^3F_4$ (450 nm), $^1D_2 \rightarrow {}^3H_6$ (362 nm), $^1I_6 \rightarrow {}^3F_4$ (345 nm) and $^1I_6 \rightarrow {}^3H_6$ (290 nm).

5. Modulation of UC emissions *via* Energy Transfer

Due to the optical property and further application value of UC emission, its modulation has always been a big concern. This manipulation of UC emissions falls into two categories, namely (a) effective enhancement for original emissions and (b) multi-color outputs regulation.

In an ETU based system, Yb^{3+} ions are usually introduced to sensitize the photon upconverting process and improve the UC efficiency, due to its relatively large absorption cross-section and suitable energy level for energy transfer. Even though, transitions from 4f-4f configurations are parity-forbidden, and the absorption cross-sections of Ln^{3+} are actually small. Moreover, non-radiative relaxations often take place simultaneously with the upward transitions. And the choices of efficient luminescent activators are limited. As shown in Fig. 5, green emission and red emission are obtained simultaneously from $Yb^{3+} - Er^{3+}$ co-doped NCs, yielding an overall yellow output. Blue emissions from $Yb^{3+} - Tm^{3+}$ co-doped NCs are the most sensitive in the visible region, giving out blue color output (Fig. 5). It is noteworthy that UC emissions from Er^{3+} (525 nm $^2H_{11/2} \rightarrow ^4I_{15/2}$, 542 nm $^4S_{3/2} \rightarrow ^4I_{15/2}$ and 655 nm $^4F_{9/2} \rightarrow ^4I_{15/2}$) and Ho^{3+} (542 nm $^5F_4$, $^5S_2 \rightarrow ^5I_8$, 655 nm $^5F_5 \rightarrow ^5I_8$) overlap heavily due to similar emission bands.[54] Such limited choices of activators and the consequent spectral similarity limit their application in multicolor encoding and multiplexed analyte detection.[23] Hence, investigations into efficient UC emissions are extremely essential.

For decades, numerous approaches have been developed to solve the above problems in order to obtain desired UC emissions, among which the delicate control of the route energy transfer is considered as the key. Ways to control energy transfer include: (a) altering energy transfer distances between sensitizers and activators; (b) introducing extraneous energy levels for novel energy transfer/multiphoton cross-relaxations; (c) incorporating energy extractors or passivators outside the luminescent UCNPs; and (d) regulating the dynamic processes of UC transitions with localized surface plasmon resonances (LSPRs) or ultra-high power excitations.
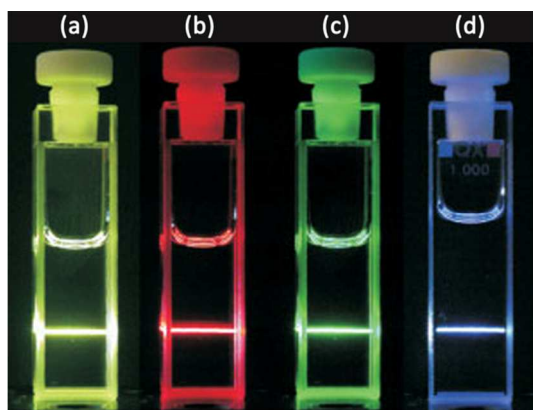
Fig. 5 Photographs of the UC luminescence in 1 wt. % colloidal solution of NCs in dimethyl sulfoxide (DMSO). (a) Total UC luminescence of the NaYF$_4$:20%Yb,2%Er sample. (b, c) Show the same luminescence through red and green color filters, respectively. (d) Total UC luminescence of the NaYF$_4$:20%Yb,2%Tm sample. (Modified with permission from ref. 43. Copyright 2004, Wiley-VCH Verlag GmbH & Co. KGaA.)

5.1 Manipulating Energy Transfer Distance

Distance between energy donor and acceptor is a key factor that affects the energy transfer efficiency significantly. In a $Yb^{3+} - Ln^{3+}$ (Ln = Er, Tm, Ho) doped ETU system, Yb^{3+} ions act as the energy donor, Ln^{3+} act as the energy acceptor. Energy transfer is completed *via* the dipole-dipole resonance between Yb^{3+} and Ln^{3+}. Resonant energy transfer efficiency is proportional to d^6, where d is the distance between donor and acceptor. Except for the influence on energy transfer efficiency, additional energy transfer pathways within dopants may occur when the distance changes. These include energy back transfer (EBT) from Ln^{3+} to the sensitizer Yb^{3+} ions, and multiphoton cross-relaxations within two adjacent Ln^{3+} ions. After distance adjustment, distinctive luminescence intensity as well as the transition with different branch ratio occur. Numerous methods have been developed to tune the distance between Yb^{3+} and Ln^{3+}, which includes controlling the lanthanide doping concentration, screening host matrix, and tailoring the local crystal field of activators.

5.1.1 controlling lanthanide doping concentration

Different doping concentration of sensitizers or activators leads to various spatial distance. Usually, the spatial distance shortens as the doping concentration increases. It has been found that the radiative transitions from high-lying excited states depend greatly on the distance of luminescent centers. As a result, distinctive color outputs with different emission intensity may be observed.

In $Yb^{3+} - Er^{3+}$ doped UC phosphors, Güdel *et al.* investigated the effect of composition on the UC emissions of Er^{3+}.[65] A general phenomenon was found that, independent of the host matrix or particle size, the UC emission intensity and R/G ratio of Er^{3+} enhanced steadily with increasing content of Yb^{3+}. An increase in the energy transfer from Yb^{3+} ($^2F_{5/2}$) to Er^{3+} ($^4I_{11/2}$) was proposed to account for the enhancement of the $^4F_{9/2} \rightarrow ^4I_{15/2}$ transition. Haase and coworkers investigated the UC properties of Er^{3+} in the $CaZrO_3$[66] and ZrO_2[67] based phosphors. They found that the green emission of Er^{3+} dominated the visible regime when there was no Yb^{3+} in the system. However, when Yb^{3+} ions were introduced, the red emission enhanced considerably and generated a yellow emission output. They held that cross-relaxation process between two nearby Er^{3+}: $^4S_{3/2} + ^4I_{15/2} \rightarrow ^4I_{9/2} + ^4I_{13/2}$ should account for the enhanced R/G ratio.

In $Yb^{3+} - Er^{3+}$ co-doped UCNPs, enhanced red emissions as a result of the increasing doping concentration of Yb^{3+} has also been reported. Capobianco *et al.* have discovered this phenomenon in nanocrystalline Y_2O_3:Yb,Er NCs in 2004.[68] Under NIR irradiation (978 nm), simultaneous green/red emission, generated *via* the excitation of Y_2O_3:Yb,Er (1%, 1%) and energy transfer from Yb^{3+} to Er^{3+}, can be obtained. However, as the doping ratio of Yb^{3+} increased, red UC emission was significantly enhanced, whilst green emission was suppressed completely when the doping concentration of Yb^{3+} reached 10%. This was attributed to the cross-relaxation of $^4F_{7/2}$

(Er^{3+}) + $^4I_{11/2}$ (Er^{3+}) → $^4F_{9/2}$ (Er^{3+}) + $^4F_{9/2}$ (Er^{3+}), where the transition from $^4F_{9/2}$ responsible for the red-emitting state. And they reported a noticeable enhancement of red emission with elevating doping concentration of Er^{3+}. Zhang *et al.* studied the relationship between the doping concentration of Yb^{3+} and the UC spectral property of α-NaYF$_4$:Yb,Er NCs.[69] When the doping ratio of Yb^{3+} increased from 0 to 10%, the red to green ratio (R/G) of emission increased from 2 to 22. This was also explained as a result of the cross-relaxation between two adjacent Er^{3+} ions.

Inspired by the absolute optical advantage of β-NaYF$_4$:Yb,Er NCs, our group studied the dependency of the UC properties on the composition of such NCs.[61] Both the doping ratio of Yb^{3+} (10 to 30 %) and Er^{3+} (0.5 to 5 %) was carefully tuned, and the corresponding UC luminesce intensity and G/R (green to red emission ratio) were monitored. For β-NaYF$_4$:Yb,Er NCs, when the concentration of Er^{3+} was fixed at 2 %, enhanced luminescence of Er^{3+} was observed with the increase of the Yb^{3+} doping ratio from 10 % to 20 %. However, when the Yb^{3+} doping ratio continued to increase from 20 % to 30 %, decrease in the emission intensity was observed. Thereby 20% was considered the optimized doping ratio of Yb^{3+} in this case. On the other hand, G/R decreased almost monotonically with the Yb^{3+} doping ratio rose from 10 % to 30 %. In another set of experiments when the doping concentration of Yb^{3+} was fixed at 20 %, the optimized Er^{3+} doping ratio for the strongest UC emission was found to be 2 %, and G/R increased monotonically with the Er^{3+} doping ratio rose from 0.5 to 5 %. Shortened energy transfer distance of high doping systems should be account for relatively enhanced red emissions.

In addition to cross-relaxation, EBT from Er^{3+} to Yb^{3+} was also considered as an important factor in high doping UCNPs. Liu and coworkers also observed the enhancement of red emissions for α-NaYF$_4$:Yb,Er NCs when the Yb^{3+} doping ratio increased from 25 % to 60%.[70] This comes from the decreased the interatomic distance between Yb^{3+} and Er^{3+}, and thus facilitated the EBT process from Er^{3+} to Yb^{3+}: $^4S_{3/2}$ (Er^{3+}) + $^2F_{7/2}$ (Yb^{3+}) → $^4I_{13/2}$ (Er^{3+}) + $^2F_{5/2}$ (Yb^{3+}). As $^4I_{13/2}$ is the intermediate state for the population of $^4F_{9/2}$, the higher domination of $^4I_{13/2}$ would result in increased probability for red emissions. In a recent report, such increase of R/G was observed for tetragonal LaOCl:Yb,Er[71] and Ba$_2$YF$_7$:Yb,Er[72] NCs for higher Yb^{3+} doping, and the observed emission changing from green to red and from green to yellow, respectively.

As for Yb^{3+} – Tm^{3+} co-doped UCNPs, a trend was also observed for the relationship between the doping ratio of Yb^{3+} and Tm^{3+} and the UC emissions. Emissions from Tm^{3+} doped UCNPs fall into three separate spectral regions in terms of wavelengths: UV (290/345/362 nm), visible (450/475/644/ 694 nm), and NIR (800 nm). It is worth mentioning that not all the emissions in the same region are derived from the same excited states. For example, the 345 nm and 362 nm emissions are generated from $^1I_6$ → $^3F_4$ (five-photon) and $^1D_2$ → $^3H_6$ (four photon) transitions, respectively. Therefore, these emissions are also categorized according to the number of photons involved
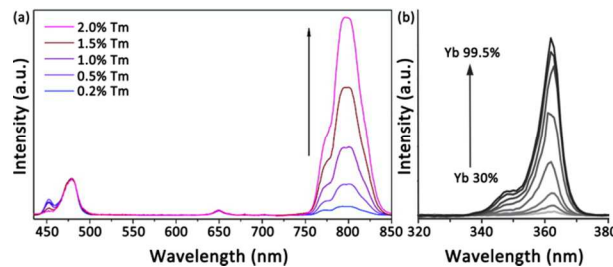
Fig. 6 (a) Room temperature UC emission spectra (normalized to Tm^{3+} 480 nm emission) of NaYF$_4$:Yb,Tm (20/0.2 − 2%) particles in ethanol solution (10 mM) under 980 nm excitation with 600 mW diode laser. (b) UV emission spectra of α-NaYF$_4$:Yb,Tm@CaF$_2$ with different Yb^{3+}-levels. a, modified with permission from ref. 70. Copyright 2008 American Chemical Society. b, modified with permission from ref. 74. Copyright 2013, Wiley-VCH Verlag GmbH & Co. KGaA.)

in that particular UC processes: five-photon (290 nm, 342 nm), four-photon (362 nm, 450 nm), three-photon (475 nm, 644 nm) and two-photon (694 nm, 800 nm) process. Based on these facts, the impact of doping concentration on UC emissions is discussed. Usually, more Yb^{3+} favors the UC emissions from Tm^{3+} due to the more efficient absorption and energy transfer from Yb^{3+} to Tm^{3+}. The concentration of Tm^{3+}, however, should also be tuned. Higher concentration would causes considerable non-radiative cross-relaxations between two adjacent Tm^{3+} ions.

Liu's group realized the facile control of the two-photon NIR emission (800 nm, $^3H_4$ → $^3H_6$) by tuning the doping ratio of Tm^{3+} while that of Yb^{3+} was fixed at 20 % (Fig. 6a).[70] Originally, α-NaYF$_4$:Yb,Tm (20 %, 0.2 %) NCs gave a weak emission at 800 nm. By increasing the Tm^{3+} ratio up to 2 %, the intensity of NIR emission remarkably increased in the emission from Tm^{3+}. This was attributed to the promoted cross-relaxation of $^1G_4$ (Tm^{3+}) + $^3F_4$ (Tm^{3+}) → $^3H_4$ (Tm^{3+}) + $^3F_2$ (Tm^{3+}) when the spatial distance between Tm^{3+} decreased. The NIR-to-NIR emission intensity could also be enhanced with increased concentration of Yb^{3+}. Prasad and coworkers observed the 8.6 times enhancement in emission intensity with an increase relative content of Yb^{3+} from 20% to 98%.[73] They attributed the enhancement to an increased absorption and energy transfer efficiency induced by decreased spatial distance between Yb^{3+} and Tm^{3+}.

Our group studied four- and three-photon UC properties *versus* the doping ratio of luminescent centers.[62] For the β-NaYF$_4$:Yb,Tm (20%, 0.2 − 5%) NCs, spectral results showed that the decrease of Tm^{3+} content from 5% to 0.2% tended to enhance the four-photon emissions (362 nm, 450nm) more than three-photon emissions (475 nm, 644 nm). As a result, the color output of overall emissions can be tuned from bright blue to purple, and to dark red. Furthermore, higher doping ratio of Yb^{3+} was also found to be more favored by four-photon emissions than tree-photon emissions, which indicated the population of high-lying excited state of $^1D_2$ at high doping ratio of Yb^{3+}. This result was confirmed by Han and his coworkers.[74] They fabricated a series of α-NaYF$_4$:Yb,Tm@CaF$_2$ NPs with the Yb^{3+} doping ratio ranging from 30 to 99.5% (Fig. 6b). Doping ratio of Tm^{3+} was kept at

0.5%, a universal adopted value. From their results, UV luminescence intensity located at 342 nm and 360 nm enhanced monotonically with increased Yb^{3+} concentration. Compared with the considerable enhancement of five and four-photon emissions, limited promotion from three- and two-photon process were observed. Such selectivity has also been observed by Qin *et al.* in $NaLuF_4$:Yb,Tm (20 – 98%, 2%) NCs[75] and Prasad *et al.* in YF_3: Yb, Tm (10 – 90%, 2%) NCs.[76]

5.1.2 screening host matrix

Host matrix provides doping sites for lanthanide luminescent centers. In most cases, the host matrix is optical inert. Apart from the adoption ability, various host matrixes do play an important role in regulation of emissions. In Eu^{3+} activated DS NCs, electric-dipole transition of $^5D_0 \rightarrow {}^7F_2$ (~ 613 nm) shows hypersensitivity to local coordination structure, while the close-lying $^5D_0 \rightarrow {}^7F_1$ emission (~ 590 nm) resulted from magnetic-dipole transition exhibited sluggishness to the alternative of host matrix. Thus we can deduce the symmetry of host matrix according to the branch ratio of Eu^{3+} emissions.[77] Similarly, luminescence intensity and branch ratio of UC emissions from Er^{3+} or Tm^{3+} also show high sensitivity to the change of host matrix. Luminescent centers doped in different host matrixes are faced with distinctive spatial distance, coordination numbers, and also energy transfer efficiency. In addition, host matrixes with different phonon energy show diverse potential to generate non-radiative relaxations through lattice vibration. Although most cross-relaxations are undesirable, branch ratio

of the emissions can be effectively regulated after the occurrence of cross-relaxations. Screening of the host matrix can be classified into two aspects: new compounds with different composition and different phase structures of the same inorganic compound.

Soukka *et al.* have comprehensively investigated host matrix decided color outputs in Yb^{3+}– Er^{3+} co-doped UCNPs.[78] A general rule can be summarized from their studies: R/G in RE based oxides and oxychlorides was apparently larger than that in oxysulfides, fluorides and fluoride double salts. Such host matrix sensitive UC emissions indicated the importance of host matrix. As listed in Table 2, we summarize recent reported Er^{3+} activated UCNPs with different host matrixes, corresponding doping ratio and color outputs. Recently, Liu and coworkers proposed a novel generation of host matrix to improve multiphoton UC emissions at 415 nm ($^2H_{9/2} \rightarrow {}^4I_{15/2}$) through energy clustering at sublattice level.[89] In Er^{3+} activated orthorhombic crystallographic KYb_2F_7 NCs, luminescent centers were distributed in arrays of tetrad clusters. Importantly, this unique arrangement enabled the preservation of excitation energy within sublattice domain and effectively minimized the migration of excitation to defects, even in high Yb^{3+} doped compounds. The significantly enhanced violet emission was regarded as four-photon UC transitions. Spectral results and proposed four-photon UC mechanism and excitation energy clustering in the Yb^{3+} tetrad clusters are shown in Fig. 7. From the proposed mechanism, enhanced violet UC emission is resulted from following transition processes. Firstly, the $^4S_{3/2}$

Table 2 Typical host matrixes doped with Yb^{3+} and Er^{3+} with corresponding relative doping ratio and color output

Host matrix	Relative Doping Ratio	Color output	Ref.	Host matrix	Relative Doping Ratio	Color output	Ref.
Y_2O_3	Yb 10%, Er 1%	Red	68	CaF_2	Yb 20%, Er 2%	Green	43
$NaYF_4$	Yb 20%, Er 2%	Yellow	43	KYF_4	Yb 20%, Er 2%	Green	80
La_2O_2S	Yb 2.7%, Er 1.6%	Green	78	YOF	Yb 20%, Er 2%	Red	81
Y_2O_2S	Yb 2.7%, Er 2.2%	Green	78	$NaScF_4$	Yb 20%, Er 2%	Red	82
YF_3	Yb 17%, Er 0.8%	Green	78	KSc_2F_7	Yb 20%, Er 2%	Red	83
YOCl	Yb 85%, Er 3.9%	Red	78	Ca_xYF_{3+2x}	Yb 22%, Er 2%	Yellow	84
Gd_2O_2S	Yb 30%, Er 7%	Green	78	$GdVO_4$	Yb 20%, Er 1%	Green	85
YbOCl	Yb 84.9%, Er 3.9%	Red	78	BiF_3	Yb 20%, Er 2%	Yellow	86
$NaYF_4$	Yb 20%, Er 2%	Green	48	$LiYF_4$	Yb 18%, Er 2%	Green	87
$KMgF_3$	Yb 20%, Er 2%	Red	78	$LiLuF_4$	Yb 20%, Er 1%	Green	88
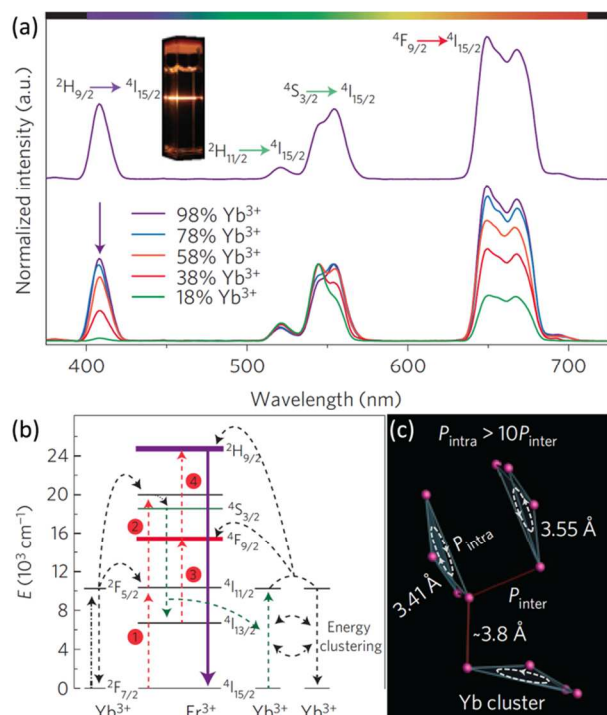
Fig. 7 (a) Room-temperature emission spectra of KYb_2F_7:Er (2%; top) and KYb_2F_7:Er/Lu (2/0–80%; bottom) NCs recorded in cyclohexane solutions (0.2 wt%). All samples were excited with a 980 nm laser at a power density of 10 W cm^{-2}. The spectra are normalized to Er^{3+} emission either at 558 nm or 545 nm, whichever is stronger. The inset is a typical micrograph showing the luminescence of KYb_2F_7:Er (2%) NCs. (b) Proposed four-photon UC mechanism in KYb_2F_7:Er (2%) NCs following excitation with a 980 nm laser. The dashed-dotted, dashed, dotted, and full arrows represent photon excitation, energy transfer, multiphoton relaxation, and emission processes, respectively. (c) Proposed excitation energy clustering in the Yb^{3+} tetrad clusters of orthorhombic-phase KYb_2F_7. The probability of energy transfer within the Yb^{3+} clusters (P_{intra}) is calculated to be more than 10 times higher than that of inter-cluster energy transfer (P_{inter}). (Modified with permission from ref. 89. Copyright 2013, Nature Publishing Group.)

state of Er^{3+} was populated by twice sequential energy transfer from neighboring Yb^{3+}. Then, the EBT process, $^4S_{3/2}$ (Er^{3+}) + $^2F_{7/2}$ (Yb^{3+}) → $^4I_{13/2}$ (Er^{3+}) + $^2F_{5/2}$ (Yb^{3+}), took place to populate the $^4I_{13/2}$ state. And localized energy transfer within the Yb^{3+} clusters provided two additional photons to Er^{3+}, leading to population of $^2H_{9/2}$ state. Finally, cascade violet emissions generated *via* $^2H_{9/2} → ^4I_{15/2}$ transition.

Apart from modulation of visible emissions, researchers also

investigated variation of UV emissions from Tm^{3+} in different host matrixes. Capobianco *et al.* have reported a type of LiYF$_4$:25%Yb,0.5%Tm NCs.[90] Although the doping ratio of Yb^{3+} is moderate, spectral results showed intense UV emissions. Zhao's group assessed the potential role of Gd^{3+} doping in NaYF$_4$:Yb,Tm NCs.[91] They discovered that strong UV emissions can be maintained after Gd^{3+} doping, typically 20%.

From Table 2, we can find that UC emissions of NaYF$_4$:Yb,Er NCs with the same concentration of luminescent centers, show distinctive branch ratios and thus present different color outputs. This should be ascribed to the two different phase structures of NaYF$_4$ NCs. As shown in Fig. 8a, b, the crystal structure of cubic and hexagonal differs completely, including spatial distance, coordination number, and symmetry of the local RE^{3+} local sites, and the spatial arrangement of RE^{3+}.[92] In the structure of α-NaREF$_4$ (RE = Ln, Sc, Y), RE^{3+} and Na$^+$ ions occupy the cation sites randomly. In contrast, the cation sites are of three types in the structure of β-NaREF$_4$: (i) a onefold site fully occupied by RE^{3+}, (ii) a onefold site randomly occupied by 1/2 RE^{3+} and 1/2 Na$^+$, and (iii) a twofold site occupied by Na$^+$ or vacancies stochastically. NCs in different crystal structures result in distinctive color outputs of Er^{3+}. Fig. 8c, d describe typical UC emissions of α-, β-NaYF$_4$:Yb,Er NCs under 980 nm excitation, respectively. As shown, green emission (525 nm $^2H_{11/2} → ^4I_{15/2}$, 542 nm $^4S_{3/2} → ^4I_{15/2}$) and red emission (655 nm $^4F_{9/2} → ^4I_{15/2}$) are both prominent in α-NaYF$_4$:Yb,Er NCs, yielding yellow output. By contrast, green emission dominates the visible regime in β-NaYF$_4$:Yb,Er NCs, thus green output is frequently observed. Also, in terms of the luminescence intensity of Er^{3+}, β-NaYF$_4$ NCs in most cases afford more than two orders of magnitude stronger emissions than the α-NaYF$_4$ counterparts.[48]

5.1.3 tailoring the local crystal field

As mentioned, the 4f-4f intra-configurational transition of Ln^{3+} is parity-forbidden in principle. However, when they are embedded in a complex or inorganic lattice, the parity forbidden rule is partially allowed due to the mixing of certain odd-parity configurations. This configurational mixing comes from the change of point symmetry of the luminescent centers. This is benefit to the 4f-4f transitions of Ln^{3+}, including UC process. Thus it is possible to modulate UC emissions by tailoring the local crystal field of luminescent centers in an inorganic host matrix. Such a tailoring effect would change the
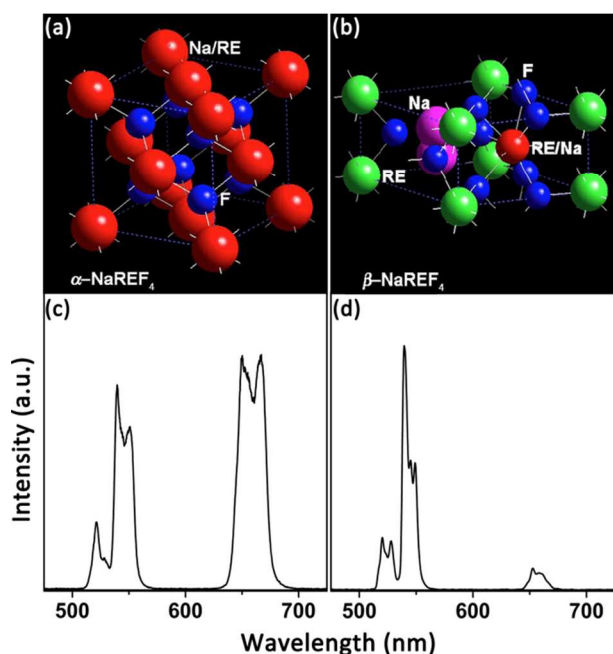
Fig. 8 (a, b) Crystal structures of α-NaYF₄ and β-NaYF₄, respectively. (c, d) Typical room temperature UC emissions of α-NaYF₄:Yb,Er and β-NaYF₄:Yb,Er NCs with normalized intensity under 980 excitation. (a, b) modified with permission from ref. 92. Copyright 2006 American Chemical Society.)

Fig. 9 (a) Measured UC spectra of NCs, bulk Y_2O_3:2%Yb,1%Er materials and Y_2O_3:5%Li,2%Yb,1%Er NCs under excitation of 970 nm. (b) Proposed UC mechanisms for green and red emissions after co-doping with Li⁺. Note that two key energy transfers, cross-relaxation (CR) and energy back transfer process (EBT) are represented as blue dashed and dashed-dotted arrows. (a, modified with permission from ref. 93. Copyright 2008 American Chemical Society)

original spatial distance between luminescent centers, generating additional multiphoton cross-relaxations and some other energy transfer processes. A quite efficient way is to compensate with other optical inert ions. Usually, the mismatch of cation size and valence state is the main consideration. Hence, several alkali metal ions and transition metal ions are frequently adopted to conduct the regulation of local crystal field.

Due to the relative smaller cationic radius, Li⁺ ions are supposed to be randomly located at the lattice site or interstices among the lattice. Such an advantage renders Li⁺ to tailor the local crystal field of the host lattice. Zhang *et al.* investigated the Li⁺ doping dependent UC properties in Y_2O_3:Yb, Er NCs for the first time.[93] They discovered significant enhancement of both green and red emissions after Li⁺ doping. Shifts of the diffraction peaks revealed the successful tailoring of local crystal field. Spectral results showed a two orders of magnitude enhancement of visible emissions by up to half of the bulk counterpart (Fig. 9a). The G/R ratio increased monotonously from 5 to 15 and kept constant approximately after the concentration of Li⁺ reached 5%. It means that tailoring of the local crystal field benefits to green emission ($^2H_{11/2} \rightarrow {}^4I_{15/2}$, $^4S_{3/2} \rightarrow {}^4I_{15/2}$) other than red emission ($^4F_{9/2} \rightarrow {}^4I_{15/2}$). To uncover the hiding mechanism, they monitored the lifetime in the $^4I_{11/2}$ (Er³⁺) and $^2F_{5/2}$ (Yb³⁺) states. From the decay curves, lifetimes of the two states prolonged. Green emission is mainly depended on the population of the $^2F_{5/2}$ (Yb³⁺) and $^4I_{11/2}$ (Er³⁺) states, while red emission is relied on the population of intermediate state of $^4I_{13/2}$ states. From these evidence, the

authors proposed the EBT $^4S_{3/2}$ (Er³⁺) + $^2F_{7/2}$ (Yb³⁺) → $^4I_{13/2}$ (Er³⁺) + $^2F_{5/2}$ (Yb³⁺) and cross-relaxation $^2H_{11/2}$(Er³⁺) + $^2I_{15/2}$(Er³⁺) → $^4I_{9/2}$(Er³⁺) + $^4I_{13/2}$ (Er³⁺) processes (Fig. 9b). Due to lengthened lifetime of $^4I_{11/2}$ (Er³⁺) and $^2F_{5/2}$ (Yb³⁺) states and extra population of the $^4I_{13/2}$ (Er³⁺) states, green and red emissions enhanced. Different G/R ratio could be attributed to the competing preference of these two aspects.

Following this tendency, enhancement of UC emissions have also been observed in other systems. UC emissions from NaYF₄:Yb,Er NCs showed more than 30-fold increase after 80% Li⁺ doping.[94] And the adding of Li⁺ into Zn_2SiO_4:Yb,Er NCs makes the up-converted green emission 6 times increasement.[95] In Yb³⁺ − Er³⁺ doped $BaTiO_3$ NCs, the incorporation of Li⁺ drastically intensified the luminescence by about 10 times compared with that of the undoped counterpart.[96] Such an enhancement was also reported for Y_2O_3:Yb,Er NCs[97] and β-NaGdF₄:Yb,Er NCs.[98] In most cases, enhancement efficiency for green emissions exhibit little superiority than that for red emissions after introduction of Li⁺. This phenomenon should be attributed to the priority of prolonged lifetimes of the $^2F_{5/2}$ (Yb³⁺) and $^4I_{11/2}$ (Er³⁺) states as well as the promoting population on the $^2F_{5/2}$ (Yb³⁺) states. Different from that, Zhao

and coworkers described an increasing R/G ratio in GdF_3:Li,Yb,Er NCs, with a color output from yellow to red.[99] They reasoned that additional population of the $^4I_{13/2}$ state (Er^{3+}) resulted from EBT, cross-relaxation processes as well as the relaxation, $^4I_{11/2}(Er^{3+}) \rightarrow ^4I_{13/2}(Er^{3+})$, within Er^{3+} ions facilitated the increased red emission.

Besides the enhancement effect for green and red emissions, tailoring of the local crystal field induced by incorporating Li^+ has also been proved to be efficient for violet and unusual UV emission of Er^{3+}. Zhang's group discovered the enhancement effect in Y_2O_3:Li,Yb,Er NCs.[100] From their opinions, after two-photon population of the $^4S_{3/2}$ and $^4F_{9/2}$ states, ESA processes takes place to further promotion to the $^4G_{11/2}$ and $^2H_{9/2}$ states, respectively, yielding UV and violet emissions through $^4G_{11/2} \rightarrow ^4I_{15/2}$ and $^2H_{9/2} \rightarrow ^4I_{15/2}$ transitions. After co-doping with Li^+, observed lengthened lifetime of the $^4S_{3/2}$ state was further involved for the enhancement of UV or violet emissions.

Interestingly, enhancement by tailoring the local crystal field can take place in Er^{3+} singly activated UCNPs without the sensitization from Yb^{3+}. Zhang et al. demonstrated the tailoring of local crystal field induced enhancement of green emissions from Er^{3+} in Y_2O_3:Er NCs.[101] Lifetime lengthening of the $^4I_{11/2}$ state directly related to the intensity increase. Sequential transition $^4I_{11/2} \rightarrow ^4F_{7/2}$ and relaxations $^4F_{7/2} \rightarrow ^2H_{11/2}$, $^4F_{7/2} \rightarrow ^4S_{3/2}$ assisted the population on the green emitting states. Two orders enhancement of green emissions was observed according to the spectral results. Song et al. discovered about 20 times enhancement in Y_2O_3:Er NCs with 3% Li^+ co-doping.[102] For ZnO:Li,Er NCs, two orders enhancement took place in 2% Li^+ doped ZnO:Er NCs.[103] In this work, the authors obtained the Er – O bond lengths and the coordination number of Er^{3+} with extended X-ray absorption fine structure spectroscopy (EXAFS). These structural parameters directly revealed the alteration in local crystal field around Er^{3+}.

As reported, symmetry tailoring can also lead to enhanced UC emissions in Tm^{3+} and Ho^{3+} activated NCs. Chen et al. discovered 10 times promotion of blue emissions ($^1D_2 \rightarrow ^3F_4$, $^1G_4 \rightarrow ^3H_6$) in Gd_2O_3:Yb,Tm NCs co-doped with 6% Li^+.[104] Song's group demonstrated 10 and 4 times increase for red ($^5F_4$, $^5S_2 \rightarrow ^5I_8$) and green ($^5F_5 \rightarrow ^5I_8$) emissions in Y_2O_3:3%Li,4%Yb,1%Ho NCs.[105]

Apart from Li^+, several transition metal ions like Bi^{3+}, Fe^{3+}, and Pb^{2+} are used to tailor the local crystal field as well. In Bi^{3+} introduced Zn_2SiO_4:Yb,Er NCs, UC luminescence intensity showed 20 times enhancement.[95] Compared with Li^+ doped spectral results, co-doped Bi^{3+} might lower the local symmetry of luminescent centers in Zn_2SiO_4 more greatly. Recently, Kim and his coworkers discovered 34 and 30 times enhancement for green and red emission intensities in β-$NaGdF_4$:Yb,Er NCs containing 30% Fe^{3+}.[106] Wang's group introduced Pb^{2+} to the synthesis of $NaYF_4$:Yb,Er NCs. With the content of Pb^{2+} increasing, β-to-α phase transition occurred as well as the change in color outputs from green to red.[107] This spectral transformation was attributed to oxygen impurities and some other potential which are resulted from the broken crystal symmetry.

In bulk materials, tailoring the local crystal field is also efficient for enhancement of UC emissions. Haase and coworkers prepared $CaAl_{12}O_{19}$:Mg,Yb,Er UC phosphors, in which the Mg^{2+} ions were supposed to replace the sites of Al^{3+} ions. As a result, the radiative relaxation probability of Er^{3+} ions was proved. Compared with the counterparts without Mg^{2+} ions, they observed a 4 and 1.5 times enhancement in the green and red emissions, respectively.[108] Recently, Yu's group employed Sn^{2+} to tune the local crystal field of $NaYF_4$:Sn,Yb,Er microrods. Enhanced UC emission intensity and reduced decay time were observed when the content of Sn^{2+} was 3%.[109]

Except for doping with optical inert non-Ln^{3+}, crystal symmetry could also be tailored by other means. In 2011, an interesting work reported by Hao et al. demonstrated the feasibility of UC luminescence enhancement and modulation by applying relatively low voltages to $BaTiO_3$:Yb,Er thin films.[110] They ascribed the unusual phenomenon to the promotion in radiative emission probabilities resulting from the lower symmetry of Er^{3+} sites, which took place after the introduction of an external electric field.

5.2 Introducing Extraneous Energy Levels

UC emissions are determined by depopulating radiative transitions from high-lying energy levels. Before an emission generates, various interactions take place orderly among the fixed energy levels, including upward transitions, energy transfers from sensitizers, and non-radiative relaxations (ETU type). In addition to the manipulation of energy transfer distances, UC processes are sure to be affected by inserting extraneous energy levels. The newly-introduced energy levels are able to interact with the native ones of original activators, leading to novel multiphoton relaxations or some other energy transfer pathways. Luminescent Ln^{3+} ions and certain transition metal ions are often introduced to alter the population and transition routes.

5.2.1 multiple Ln^{3+} ions activation

Distinctive energy levels endow lanthanides with unique spectral fingerprints differed from others. Multicolor outputs could be produced in multiple Ln^{3+} ions activated UCNPs. Meanwhile, novel interactions among activators are likely to take place to regulate the populations or lifetimes on emissive high-lying excited states. These interactions usually occur via multiphoton cross-relaxation processes or direct energy transfers (sensitization) from one to another. After various energy transfer pathways, novel emission bands or altered emission branch ratios are able to be detected from the UC spectra.

Xu et al. synthesized a series of $NaYbF_4$ based NCs doped with Er^{3+}, Tm^{3+}, Ho^{3+}, as well as $Er^{3+} - Tm^{3+}$, $Tm^{3+} - Ho^{3+}$ and $Er^{3+} - Ho^{3+}$ pairs, respectively (Fig. 10).[111] As shown, the emission outputs were obviously tuned after doping with another type of activator. This indicated that multicolor emission behaviors could be tuned with co-doping. Liu's group elaborated UC multicolor fine-tuning in the visible region in a three-component dopant system (α-$NaYF_4$:Yb,Er,Tm).[70] Prior
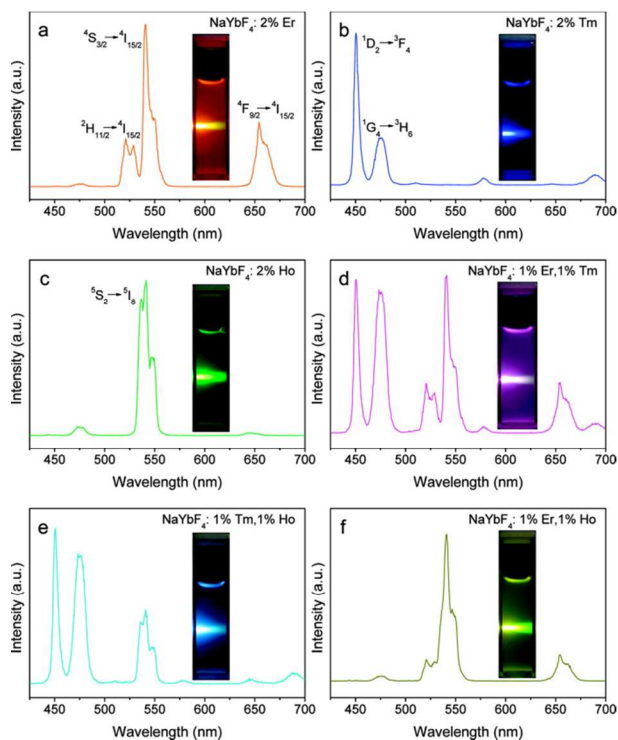
Fig. 10 UC spectra of 1 wt% colloidal solutions of NaYbF$_4$:Ln@SiO$_2$ NCs in water excited with a 980 nm laser. Ln = 2% Er (a), 2% Tm (b), 2% Ho (c), 1% Er + 1% Tm, (d) 1% Er + 1% Tm, (e) 1% Tm + 1% Ho, (f) 1% Er + 1% Ho. Insets are the digital photographs of 1 wt% colloidal solutions of corresponding NCs in water, excited with a 980 nm laser. (Modified with permission from ref. 111. Copyright 2009 American Chemical Society)

to Er^{3+} doping, an overall blue color output was observed in α-NaYF$_4$:Yb,Tm NCs *via* $^1D_2 \rightarrow {}^3F_4$ (450 nm), $^1G_4 \rightarrow {}^3H_6$ (475 nm) and $^1G_4 \rightarrow {}^3F_4$ (644 nm, weak) transitions. By introducing Er^{3+} simultaneously, the relative intensity ratio of the two activators can be finely modulated. With a subtle increasing concentration of Er^{3+} from 0.2% to 1.5%, prominent green ($^2H_{11/2} \rightarrow {}^4I_{15/2}$, $^4S_{3/2} \rightarrow {}^4I_{15/2}$) and red ($^4F_{9/2} \rightarrow {}^4I_{15/2}$) emissions arose in the visible spectral region, accompanied by a slight change in the violet emission ($^2H_{9/2} \rightarrow {}^4I_{15/2}$). Consequently, color outputs of α-NaYF$_4$:Yb,Er,Tm (20%, 0.2% − 1.5%, 0.2%) colloidal solutions exhibited gradual variation from blue to white. Then they reported a similar enhancement of green and red emissions of Er^{3+} in LiYF$_4$:Yb,Er,Tm (20%, 0 − 1%, 0.2%) NCs.[87] The emission outputs varied from blue to green. Moreover, modulation of the visible spectral region could also be realized by introducing Ho^{3+} to Tm^{3+} activated system. Green ($^5F_4$, $^5S_2 \rightarrow {}^5I_8$) and red ($^5F_5 \rightarrow {}^5I_8$) emissions from Ho^{3+} sharply emerged compared without Ho^{3+} counterpart.

Lin and coworkers investigated component dependent UC properties in tri-doped BaYF$_5$:Yb,Er,Tm NCs.[112] Blue emissions ($^1D_2 \rightarrow {}^3F_4$, $^1G_4 \rightarrow {}^3H_6$) enhanced gradually with the increasing concentration of Yb^{3+}. They attributed this to the improved energy transfer efficiency from Yb^{3+} to Tm^{3+} as the spatial distance shortened. White light output was obtained in BaYF$_5$:40%Yb,0.5%Er,0.5%Tm NCs under 980 nm laser excitation. Hao *et al.* described color-tunable UC emission in Yb^{3+} − Er^{3+} − Tm^{3+} tri-doped ferroelectric BaTiO$_3$ materials.[113]

They assessed the role of luminescent centers in overall color output. In BaTiO$_3$:2%Yb, 0.1%Er, 0.2% Tm phosphors, green and red emissions of Er^{3+} dominated the visible region. Increasing concentration of Yb^{3+} or decreasing content of Er^{3+} facilitated the branch ratio of blue ($^1D_2 \rightarrow {}^3F_4$, $^1G_4 \rightarrow {}^3H_6$) and red ($^3F_2$, $^3F_3 \rightarrow {}^3H_6$) emissions from Tm^{3+}.

Apart from frequently-used Er^{3+}, Tm^{3+} and Ho^{3+}, spectral combination have also been reported in Tb^{3+} and Eu^{3+} containing UCNPs. Qiu *et al.* introduced Tb^{3+} into Ba$_2$LaF$_7$:Yb,Tm NCs,[114] and the UC spectra showed typical Tb^{3+} green emission ($^5D_4 \rightarrow {}^7F_5$). Moreover, enhancement in Tb^{3+} emission intensity and descending in Tm^{3+} emission intensity ($^1G_4 \rightarrow {}^3H_5$) were discovered with the increasing concentration of Tm^{3+}, indicating the occurrence of energy transfer from Tm^{3+} ($^1G_4$) to Tb^{3+} ($^5D_4$). Qin's group reported unusual transitions of Eu^{3+} in Yb^{3+} − Er$^{3+} \rightarrow$ Eu^{3+} tri-doped NaYF$_4$ NCs.[115] Energy acquired from adjacent Er^{3+} rendered $^5D_J \rightarrow {}^7F_{J'}$ transitions (J = 0, 2, 3; J' = 0 − 3) transitions of Eu^{3+}.

With multiple Ln^{3+} activation, the emission colors could also tuned easily in bulk materials. Gouveia-Neto *et al.* successfully obtained the red, green, blue, and white light colors in germanate glass by selectively doping with Yb^{3+}, Ho^{3+}, and Tm^{3+}.[116] Wang *et al.* obtained the white light output in LiNbO$_3$ single crystals by tri-doping with Yb^{3+}, Ho^{3+}, and Tm^{3+}. Moreover, they tuned the colors simply by changing the 980 nm excitation power.[117] Later, the authors demonstrated that the UC emissions from the LiNbO$_3$:Yb,Ho,Tm single crystal could also be regulated by changing the temperature.[118] Such temperature dependent UC property made the LiNbO$_3$:Yb,Ho,Tm single crystal applicable for temperature sensing.

Multiple Ln^{3+} ions activation can not only result in novel emission bands from the activators, but also change emission branch ratio of the native counterpart. Such a managed ability mainly derives from mutual multi-photon cross-relaxations. Zhang's group achieved successful UC emission tuning from Ce^{3+} under 970 nm excitation.[119] As shown in Fig. 11a, two efficient multiphoton cross-relaxation processes between Ce^{3+} and Ho^{3+} have been employed to select UC pathways to tune the visible radiation: $^5I_6$ (Ho^{3+}) + $^5F_{5/2}$ (Ce^{3+}) $\rightarrow {}^5I_7$ (Ho^{3+}) + $^2F_{7/2}$ (Ce^{3+}) and $^5S_2/^5F_4$ (Ho^{3+}) + $^5F_{5/2}$ (Ce^{3+}) $\rightarrow {}^5I_5$ (Ho^{3+}) + $^2F_{7/2}$ (Ce^{3+}). Red emissions ($^5F_5 \rightarrow {}^5I_8$) gradually dominated the visible spectral region with an increase Ce^{3+} concentration from 0 to 15%. Decreased NIR emission intensity of $^5I_6 \rightarrow {}^5I_8$ transitions, as well as the deteriorative decay time of $^5F_4$, $^5S_2 \rightarrow {}^5I_8$ transitions of Ho^{3+} suggested the occurrence of proposed cross-relaxations. Li *et al.* also studied the effect of Ce^{3+} on UC emissions of Ho^{3+}. By tri-doping with Ce^{3+}, an increase in the intensity of red emission relative to green was detected. More importantly, unusual $^5G_5 \rightarrow {}^5I_7$ and $^5F_2/^5K_8 \rightarrow {}^5I_8$ transitions from Ho^{3+} and 5d $\rightarrow$ 4f transitions from Ce^{3+} were observed. They announced the phenomenon for the same reason.[120]

The former two studies indicate the importance of cross-relaxations in UC emissions. Actually, efficient cross-relaxations can take place in other lanthanide pairs, for example, Er^{3+} − Tm^{3+}. Qin et al. demonstrated the successful modulation
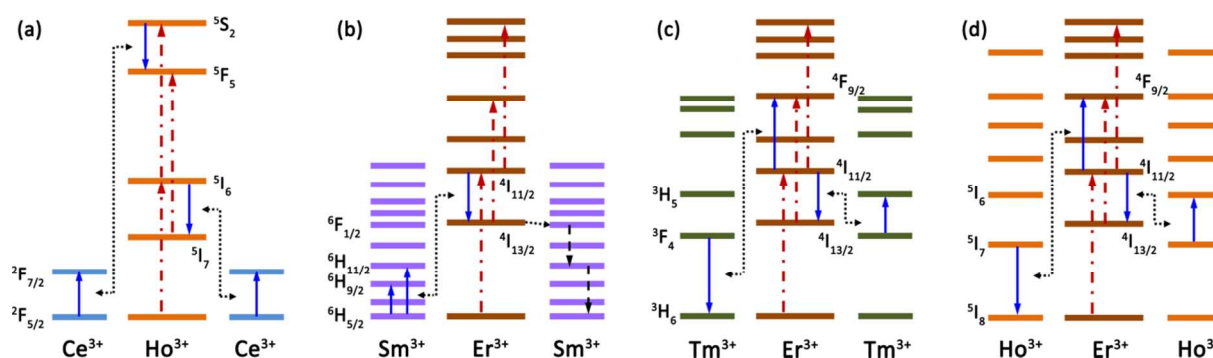
Fig. 11 Typical energy transfer pathways for UC emission modulation. Multiphoton cross-relaxations generated between (a) Ce^{3+} – Ho^{3+} pairs (ref. 119), (b) Er^{3+} – Sm^{3+} pairs, (c) Er^{3+} – Tm^{3+} pairs, (d) Er^{3+} – Ho^{3+} pairs (ref. 122). Note that the dashed-dotted, dotted, dashed, and full arrows represent upward transitions, multiphoton cross-relaxations, non-radiative relaxations and energy transfers, respectively. Only partial energy levels of Ln^{3+} are shown for clarity.

of visible emissions from Er^{3+} doped $NaYF_4$ NCs by introducing Tm^{3+}.[121] Spectral results showed that green emission ($^2H_{11/2} \rightarrow {}^4I_{15/2}$, $^4S_{3/2} \rightarrow {}^4I_{15/2}$) decreased apparently with the introduction of Tm^{3+} while red emission ($^4F_{9/2} \rightarrow {}^4I_{15/2}$) enhanced prominently. A non-radiative cross-relaxation process was proposed to disclose the enhanced red to green emission ratio: $^3F_4$ (Tm^{3+}) + $^4I_{11/2}$ (Er^{3+}) $\rightarrow$ $^3H_6$ (Tm^{3+}) + $^4F_{9/2}$ (Er^{3+}). Such a process could generate additional population of $^4F_{9/2}$ states of Er^{3+}, yielding enhanced red emissions as a result. The intensity quenching of green UC emission was regarded as considerable depopulation from $^4I_{11/2}$ according to the proposed cross-relaxation process.

In a recent demonstration, Chan and coworkers developed a kinetic model that provided microscopic insight into the energy transfer pathways that result in spectrally pure emission in multiply doped UCNPs.[122,123] Combinatorial spectral results showed that green emission dominated spectra could be generated from Er^{3+} – Pr^{3+} and Er^{3+} – Sm^{3+} co-activated UCNPs, while nearly pure red emissions were discovered in Er^{3+} – Ho^{3+} and Er^{3+} – Tm^{3+} doped counterparts. Novel energy transfer pathways for spectrally pure emissions are shown in Fig. 11 b – d. Sm^{3+} suppressed the population of $^4F_{9/2}$ by depopulating the $^4I_{11/2}$ and $^4I_{13/2}$ manifolds by factors of 10 and 70 *via* energy transfer, respectively. The seriously quenched $^4I_{31/2}$ state, which is the intermediate state for red emission, results in nearly pure green emissions. Rather than selective quenching, cross-relaxations of $^4I_{11/2}$ (Er^{3+}) + $^3F_4$ (Tm^{3+}) $\rightarrow$ $^4I_{13/2}$ (Er^{3+}) + $^3H_5$ (Tm^{3+}) and $^3F_4$ (Tm^{3+}) + $^4I_{11/2}$ (Er^{3+}) $\rightarrow$ $^3H_6$ (Tm^{3+}) + $^4F_{9/2}$ (Er^{3+}), played the key role in spectrally pure red emission. Similarly, selectively enhancing population in red-emitting related states $^4F_{9/2}$ and $^4I_{13/2}$: $^4I_{11/2}$ (Er^{3+}) + $^5I_7$ (Ho^{3+}) $\rightarrow$ $^4I_{13/2}$ (Er^{3+}) + $^5I_6$ (Ho^{3+}) and $^5I_7$ (Ho^{3+}) + $^4I_{11/2}$ (Er^{3+}) $\rightarrow$ $^5I_8$ (Ho^{3+}) + $^4F_{9/2}$ (Er^{3+}) accounted for achieving pure red emission as Ho^{3+} introduced into $NaYF_4$:Er NCs.

5.2.2 mediation by transition metal ions

In recent years, several transition metal ions have been tested and verified the feasibility of UC properties under excitation by NIR photons, to name only a few, Mn^{2+},[124] Mo^{3+},[125] Re^{4+},[126] and so forth. Credit should be given to the splitting of *d* orbitals

mediated by crystal field. Except for the employment of UC activators, transition metal ions have also been introduced to Ln^{3+} activated NCs to mediate energy transfer pathways. Among the mentioned transition metal ions, Mn^{2+} is popular used for its unique $^4T_1$ state, which lies between the $^4S_{3/2}$ and $^4F_{9/2}$ states of Er^{3+}.

Li's group described a type of nanomaterials with Mn^{2+} ions dominant in the host matrix.[127] Compared with the yellowish-green emitting $KZnF_3$:Yb,Er, $KCdF_3$:Yb,Er, and $KMgF_3$:Yb,Er NCs, the R/G ratio of $KMnF_3$:Yb,Er NCs increased sizably. As a result, nearly spectrally-pure red UC emissions generated. Considering that the energy of the $^4S_{3/2}$ state lies above the $^4T_1$ excited level, the excited $^4S_{3/2}$ state would relax to a neighboring Mn^{2+} by energy transfer. Subsequently, an energy back transfer to the lower-lying $^4F_{9/2}$ state of Er^{3+} took place from Mn^{2+}. Increasing population on the red-emitting $^4F_{9/2}$ state of Er^{3+} promoted red emissions. Yu *et al*. also discovered similar enhanced red emission output from MnF_2:Yb,Er NCs compared with $NaYF_4$:Yb,Er counterpart.[128] Liu and coworkers extended the Mn^{2+} mediated energy transfer pathways to Ho^{3+} and Tm^{3+} activated UCNPs.[129] As shown in Fig. 12, spectrally pure emissions could be obtained in $KMnF_3$:Yb,Er, $KMnF_3$:Yb,Ho and $KMnF_3$:Yb,Tm NCs. Insets are detailed energy transfer pathways. Similar to $Yb^{3+} \rightarrow Er^{3+} \rightarrow Mn^{2+} \rightarrow Er^{3+}$ energy transfer style, the $^4T_1$ state of Mn^{2+} could also extract energy from $^5F_3$ and $^5F_4$ states of Ho^{3+}, and subsequently donate the absorbed energy back to the $^5F_5$ state of Ho^{3+}. Persistent depopulation of the $^5F_4$ state facilitated elimination of green emission. Meanwhile, continuous population of the $^5F_5$ state favored enhancement of red emission. As for Tm^{3+}, after the population to high-lying $^1G_4$ and $^1D_2$ states, energy transfer pathways could be described as follows: $^1D_2/^1G_4$ (Tm^{3+}) + $^6A_1$ (Mn^{2+}) $\rightarrow$ $^3H_5/^3H_6$ (Tm^{3+}) + $^4T_1$ (Mn^{2+}), $^4T_1$ (Mn^{2+}) + $^3H_6$ (Tm^{3+}) $\rightarrow$ $^6A_1$ (Mn^{2+}) + $^3F_2$ (Tm^{3+}). Afterwards, a relaxation occurred from $^3F_2$ state to $^3H_4$ state, yielding pure 800 nm emission as a result. In a follow-up study, Tan and coworkers demonstrated pure intense red emission from $NaMnF_3$:25%Yb,25%Er NCs.[130]

Apart from host lattice construction, Mn^{2+} ions have also been introduced as dopants to optical inert inorganic matrix. In
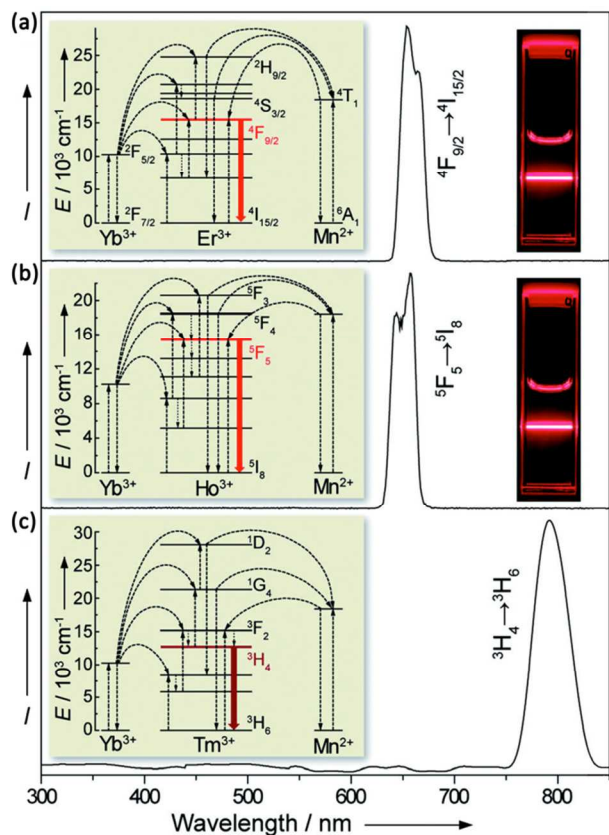
Fig. 12 Room temperature UC emission spectra of solutions containing (a) $KMnF_3$:Yb,Er (18%, 2%), (b) $KMnF_3$:Yb,Ho (18%, 2%), and (c) $KMnF_3$:Yb,Tm (18%, 2%) nanocrystals in cyclohexane (insets: proposed energy transfer mechanisms and corresponding luminescent photos of the colloidal solutions). All spectra were recorded under excitation of a 980 nm CW diode laser at a power density of 10 W cm^{-2}. (Modified with permission from ref. 116. Copyright 2004, Wiley-VCH Verlag GmbH & Co. KGaA.)

these systems, spectrally pure red emissions could also be observed. Zhao *et al*. investigated Mn^{2+} content dependent UC properties.[131] With the increasing concentration of Mn^{2+} from 0 to 30%, the R/G ratio gradually increased from 0.83 to 163.78. In further experiments, they found that the single-band feature of the 30% Mn^{2+}-doped $NaYF_4$ NCs was independent of the amount of Yb^{3+} (0 – 28%), excitation laser power and environmental temperature, thus confirming the highly efficient energy transfer process between Er^{3+} and Mn^{2+}. Zeng and co-workers realized simultaneous phase/size manipulation, UC luminescence purification and enhancement by Mn^{2+} doping into $NaLuF_4$:Yb,Er NCs.[132] The R/G ratio reached 10 or so in $NaLuF_4$:40%Mn,18%Yb,2%Er NCs.

As proved, Mo^{6+} is another efficient active transition metal ion to modulate UC emission of Ln^{3+}.[133,134] In Er^{3+} activated $Yb_3Al_5O_{12}$ (YbAG) NCs, weak red emission ($^4F_{9/2} \rightarrow {}^4I_{15/2}$) dominated UC spectra could be measured. After co-doping with Mo^{6+}, considerably enhanced green emission ($^2H_{11/2}$, $^4S_{3/2} \rightarrow {}^4I_{15/2}$) was observed. Similarly, 4 orders of magnitude enhancement of blue emission ($^1G_4 \rightarrow {}^3H_6$) occurred in Tm^{3+} – Mo^{3+} doped YbAG NCs. As a result, quantum yield of Er^{3+} and Tm^{3+} increased from 0.33×10^{-4}% to 0.2% and from 0.17×10^{-4}% to 0.18%, respectively. The authors pointed out the dimers

formed by Yb^{3+} and MoO_4^{2-} ions are responsible for the considerable sensitization. Energy levels of the $Yb^{3+} - MoO_4^{2-}$ dimer were classified into ground state $|^2F_{7/2}, {}^1A_1>$, intermediate state $|^2F_{5/2}, {}^1A_1>$ and higher excited state $|^2F_{7/2}, {}^3T_{1,2}>$ and $|^2F_{7/2}, {}^1T_{1,2}>$. Sequential absorption of NIR photons would take place from the ground state to high-lying excited state. Thus direct energy transferred from excited states to nearby $^4F_{7/2}$ (Er^{3+}) and $^1G_4$ (Tm^{3+}) states resonantly, yielding enhanced UC emissions. Besides, they demonstrated stronger UC emissions from Er^{3+} sensitized by $Yb^{3+} - Mn^{2+}$ dimers.[135]

5.3 Incorporating Energy Extractors or Passivators

UC emissions can be modulated by incorporating energy extractors or passivators decorated on the surface of nanoparticles. As the nomination implies, energy extractors would capture partial energy from activators doped in the system, resulting in decreased emission intensity. Further, certain luminescent energy extractors could give out novel emission bands after the inter-particle energy transfer. For energy passivators, they could minimize excitation energy loss induced by surface effects and solvents, leading to increased emission intensity as a result. Energy extractors can be not only intrinsic surface defects, capping ligands, but also extrinsically grafted organic dyes, quantum dots or noble metal NCs. Energy passivators are mainly devoted by epitaxial shell layers.

5.3.1 surface effects

Surface effects refer to surface related factors, which are involved in the UC emission modulation, including particle size, surface defects, and capping ligands. UC properties can be influenced greatly by the variation of the particle size. It is worth noting that emissions bands would not shift with the surface effects. Instead, the branch ratio, emission intensity, and the decay rate of the UC emissions can be affected by surface factors.

Capobianco *et al*. discovered larger branch ratio of red ($^4F_{9/2} \rightarrow {}^4I_{15/2}$) to green emission ($^2H_{11/2}$, $^4S_{3/2} \rightarrow {}^4I_{15/2}$) in nanocrystalline Y_2O_3:Yb,Er NCs than bulk counterpart.[68] This phenomenon has also noticed by Song *et al*.[136] They attributed the increasing R/G ratio to non-radiative relaxations. For red emission, the non-radiative relaxation of $^4I_{11/2}$ (Er^{3+}) $\rightarrow {}^4I_{13/2}$ (Er^{3+}) or the $^4F_{7/2}$ (Er^{3+}) + $^4I_{11/2}$ (Er^{3+}) $\rightarrow {}^4F_{9/2}$ (Er^{3+}) + $^4F_{9/2}$ (Er^{3+}) is involved in the size-dependent UC emission. As the particle size decreased, due to the increase ratio of surface to volume, plentiful surface defects with available large vibrational modes are involved, such as CO_3^{2-} (1500 cm^{-1}) and OH^- (3350 cm^{-1}), which resulted in considerable non-radiative relaxations. On the other hand, $^4I_{13/2}$ (Er^{3+}) $\rightarrow {}^4F_{9/2}$ (Er^{3+}) is nonresonant with the 980 nm excitation, thus excess energy would be dissipated by the host lattice, especially in matrixes with larger phonon vibrational energy (Y_2O_3: ~ 600 cm^{-1}). As a result, the red emission increased greatly.

We studied UC spectra of differently sized α-$NaYF_4$:Yb,Er and β-$NaYF_4$:Yb,Er NCs.[61] As the size of α-$NaYF_4$:Yb,Er nanopolyhedra decreased from 13.7 to 8.0 nm, the R/G ratio decreased from 1.59 to 2.33. As the nanopolyhedra shrank to

5.1 nm, the R/G ratio significantly decreased to 7.69 with an intense red emission. From the diagram of R/G ratio versus the size of β-NaYF$_4$:Yb,Er NCs, it could be seen that the R/G ratio decreased from 0.14 to 0.06 as the size increased from 20.2 nm to 72.1 nm.

In addition to the influence on branch ratio, change in the particle size also has an effect on the emission intensity and corresponding decay time. Krupke's group performed quantitative measurement of UC emission efficiency based on the use of a calibrated integrating sphere. They discovered that the Yb^{3+} – Er^{3+} doped green bulk phosphors were most efficient with an efficiency value of 4%, while the Yb^{3+} – Er^{3+} doped red ones and the Yb^{3+} – Tm^{3+} doped blue ones gave 1% – 2%.[137] Recently, van Veggel and co-workers employed the commercially available fluorometer and integrating sphere to measure the quantum yields of NaYF$_4$:20%Yb,2%Er with various particle sizes. The quantum yield in the range of 0.005% to 0.3% were obtained with sizes ranging from 10 to 100 nm, while the quantum yield of 3% was measured for bulk materials, which was similar with that reported by Krupke *et al*. Therefore, we can conclude that the UC emission efficiency in nanomaterials was less than that in bulk materials due to the surface effects induced by large surface-to-volume ratio.[138] Jin and coworkers presented a comprehensive analysis of the particle size dependent UC luminescence decay rates.[139] From their studies, decay time shortened monotonously with the decrease of particle size. They reasoned that such a phenomenon was dependent on the surface-to-volume ratio, and atomic-scale mechanisms such as non-radiative recombination mediated by phonons, vibrations of surface ligands, solvent mediated quenching and surface defects. Recently, Ohishi's group described similar size dependent UC luminescence.[140] As the particle size changing from 16 to 20 nm, the quantum efficiency for UC emissions increased from 0.04% to 2.1%.

Capping ligands on the surface of NCs do affect the UC emission considerably. Wu's group investigated capping ligands dependent UC emissions with a fixed composition of NaYF$_4$:20%Yb,2%Er NCs.[141] By changing the ratio of three pairs of mixtures, namely octadecylamine (OM), oleic acid (OA) and *N*-octadecyloleamide (OOA), which can be simply achieved by controlling the composition during the synthesis, the color output could be subtly tuned from green to red. In another research, a series of carboxylic acids with different carbon chain lengths have been successfully used as capping ligands in synthesis of β-NaYF$_4$:Yb,Er/Tm NCs.[142] Because relative long carbon chain length (CH$_2$)$_n$ resulted in higher energy stretching vibration, the spectral results also indicates a relative greater quenching effect from long chain ligand.

Capobianco and coworkers developed a facile strategy to modify the UCNPs from hydrophobic to hydrophilic.[143] Oleate-capped NaYF$_4$:Yb,Er NCs were treated with HCl at pH 4, which protonated the oleate ligand resulting in the release of oleic acid from the surface. As shown in Fig. 13, a drastic change took place after the surface modification. The UC emission intensity was higher for the oleate-free NCs dispersed in H$_2$O/D$_2$O compared with the oleate-capped counterpart in
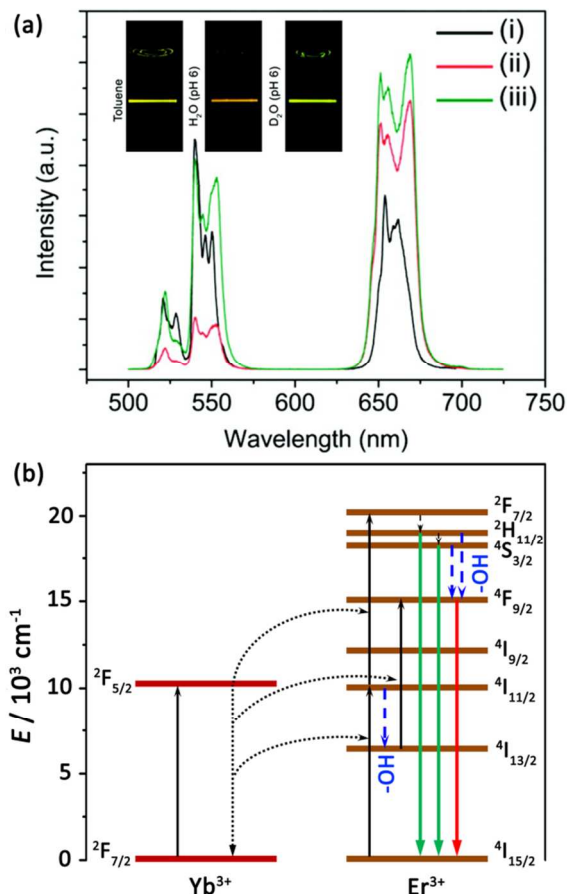
Fig. 13 (a) Upconversion luminescence spectra of (i) oleate-capped UCNPs in toluene, (ii) Oleate-free UCNPs in H$_2$O at pH = 4, and (iii) Oleate-free UCNPs in D$_2$O at pD = 4 upon excitation at 980 nm. Insets show the change in R/G ratio, which is clearly visible to the naked eye. (b) Schematic representation of the UC mechanisms in Er^{3+}/Yb^{3+} co-doped NaYF$_4$ NCs. Note that two key relaxations relative to population of red-emitting $^4F_{9/2}$ and intermediate $^4I_{13/2}$ states are presented by blue dashed arrows. (a, modified with permission from ref. 143. Copyright 2011 American Chemical Society)

toluene. Equally striking is the fact that the R/G ratio was significantly affected with the change of dispersed medium. UCNPs dispersed in H$_2$O exhibited an enhanced red remission and a decreased green emission. On the contrary, both red and green emissions increased considerably. It is supposed that the vibration of the hydroxyl group (–OH) played the key role in altering the UC emission intensities. As mentioned earlier, the $^4F_{9/2}$ state of Er^{3+} is populated through two channels: relaxation from $^2H_{11/2}$ and $^4S_{3/2}$ states as well as upward transition *via* $^4I_{13/2}$ → $^4F_{9/2}$ process. Energy gap between $^2H_{11/2}$ ($^4S_{3/2}$) and $^4F_{9/2}$ states is approximately 3200 cm^{-1}. On the other hand, –OH groups generate high-energy vibrational modes at 3200 – 3600 cm^{-1}. Hydroxyl groups on the surface increased the probability of multi-photon relaxation $^2H_{11/2}$, $^4S_{3/2}$ (Er^{3+}) → $^4F_{9/2}$ (Er^{3+}), resulting in stronger red emission and weaker green emission. Moreover, the energy gap between the $^4I_{11/2}$ and $^4I_{13/2}$ levels is approximately 3600 cm^{-1}, indicating additional population on the intermediate state of $^4I_{13/2}$ *via* resonance with vibration of –OH groups. As the –OD stretching vibrations is situated at 2600

cm^{-1}, the multi-photon relaxation processes are obviously minimized in D$_2$O solution.

5.3.2 surface passivation – core/shell nanostructure

Luminescence quenching from surface can be solved by forming a uniform shell over the core. After the epitaxial growth of shell layer, energy transfer from activators in the core to surface defects, capping ligands, and solvent molecules is blocked. And the quenching effects can thus be significantly suppressed, resulting in improved emissions. For a perfect growth of a shell, it should similar in composition, structure or lattice constant with that of the core. In recent studies, luminescent centers have been introduced into the shell layer to realize efficient sensitization and novel energy transfer that undergone through the core and shell. By this token, core/shell nanostructures can be classified into active-core/inert-shell and active-core/active-shell.

Our group investigated the shell effect on UC emissions.[61] Spectral results showed obvious enhancement in the overall emission intensity, as well as a decreased R/G ratio of Er^{3+}. The color output changed from yellow to yellowish-green as a result. Such a diverse effect could be attributed to the decrease of non-radiative relaxations which are involved in red emission. Schäfer and coworkers synthesized a series of KYF$_4$:Yb,Er@KYF$_4$ NPs with size increased from 13 to 15.5 nm.[144] The epitaxial shell improved the UC emission efficiency by more than a factor of 20. And the increased UC emission intensity and decay time for NaYF$_4$:Yb,Er@NaYF$_4$ NCs was reported.[145] YOF shell also benefit to the emission enhancement of YOF:Yb,Er NCs.[81]

Core/shell structure is also used to elucidate the surface quenching effect associated with the size-dependent luminescence of NCs.[146] An example was given for NaYF$_4$:Yb,Tm NCs. By comparing the branch ratio of blue to NIR emission intensity, the overall emission intensity before and after the shell growth, and the quenching effect induced by vibration of –OH groups, an inert thin-shell was proved to preserve the optical integrity of the NCs and largely minimized surface quenching induced emission losses. Recently, Chen's group fabricated CaF$_2$:Yb,Er/Tm@CaF$_2$ nanostructures, maximum enhancement factors were reported as 92 and 1700 for Er^{3+} and Tm^{3+} activated core NCs, respectively.[147]

Besides homogenous shell, a heterogeneous shell can passivate the core effectively as well. Such a heterogeneous shell could be distinguished with the core *via* X-ray photoelectron spectroscopy (XPS)[148] and electron energy loss spectroscopy (EELS) line scan.[149] Recently, a novel Ostwald ripening method were developed to epitaxial growth shell layer-by-layer on NaYF$_4$:Yb,Er NCs.[150] With the thickness of the shell layer increased gradually, the luminescence intensity enhanced steadily. Zhang *et al*. employed cryo-transmission electron microscopy (cryo-TEM), rigorous EELS and high-angle annular dark-field (HAADF) techniques to clarify the NaYF$_4$:Yb,Er@NaGdF$_4$ nanostructures.[151] They reported that the upconversion emission is linearly dependent on the shell thickness.

Our group developed a novel generation of core/shell nanostructure, α-NaYF$_4$@CaF$_2$.[152] Successful growing of the CaF$_2$ layer over α-NaYF$_4$ NCs should be ascribed to the same space group ($Fm\overline{3}m$) and similar lattice constants, that is, a = 5.448 Å for α-NaYF$_4$ and a = 5.451 Å for CaF$_2$. Thickness of the shell layer was precisely tuned. When the shell thickness reached *ca*. 3 nm (molar ratio of [Ca]/[RE] was 4:1), the integrated intensity of total emissions were about 300 times compared to that of the core. As shown in Fig. 14, two orders of magnitude enhancement was obtained with the CaF$_2$ shielding. Significant enhancement of UC emissions from Tm^{3+} and Ho^{3+} were also demonstrated. It is worth mentioning that suppression of RE ions leakage is also a striking progress. In a follow-up study, Bednarkiewicz and coworkers reported up to 40 fold enhancement of α-NaYF$_4$:Yb,Tb@CaF$_2$ NCs in comparison with the bare core counterpart.[153]

We can find that the epitaxial shells are sure to enhance the UC emissions of the core counterparts, however, the enhancement factors differ greatly when adopting different core/shell nanostructures. This should be ascribed to the difference in the host matrixes, as well as the thickness of the shell layers. Thicker fluorides based shell layers are considered as more excellent surface passivators.

In recent years, active-core/active-shell nanostructures have been springing up to yield more efficient passivation and creative energy transfer pathways. Capobianco and coworkers proposed the NaGdF$_4$:Yb,Er@NaGdF$_4$:Yb active-core/active-shell nanostructure to enhance the intensity of UC emissions,[154] and an increased factor of approximately 3 in the green and 10 in the red compared to the inert-shell NCs was reported. Sizable enhancement was due to extra energy transfer from Yb^{3+} embedded in the shell layer to Er^{3+} in the core. With a NaYF$_4$:Yb,Er@NaYF$_4$:Yb@NaYF$_4$:Yb,Er@NaYF$_4$:Yb four-layered core/shell nanostructure, the concentration quenching threshold of UC luminescence was broken for the first time.[155] The upper limit of the concentration quenching threshold reached 5% for Er^{3+}.
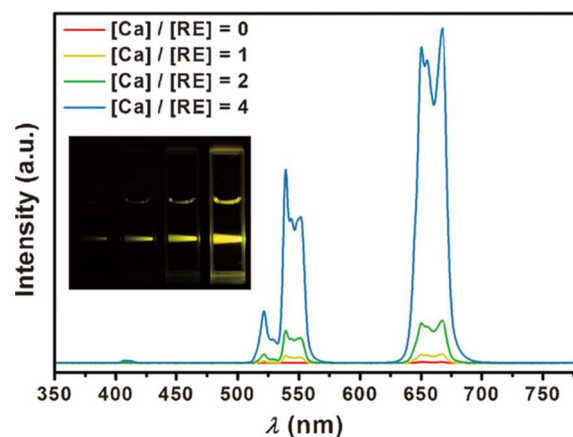
Fig. 14 UC luminescence spectra and digital photographs (inset) of α-NaYF$_4$:Yb,Er☐and☐α-NaYF$_4$:Yb,Er@CaF$_2$ NCs. Note that insets of photographs (from left to right) correspond to [Ca]/[RE] molar ratios of 0:1, 1:1, 2:1, and 4:1.(Reprinted with permission from ref. 152. Copyright 2012, Wiley-VCH Verlag GmbH & Co. KGaA.)

To minimize undesirable multiphoton cross-relaxations, Zhang *et al*. synthesized multi-layered NCs by incorporating Er^{3+} and Tm^{3+} into separated layers.[156] Independent emissions from individual activators were observed. In a recent report, an improved core/shell/shell nanoarchitecture with an energy-accumulating matrix sandwiched between the active layers was explored. [157] A $NaYbF_4$ matrix is assigned as middle layer for maximum energy absorption. In this way, they obtained efficient multicolor outputs ranging from blue to orange with differently designed UCNPs. Very recently, Liu and coworkers demonstrated a multicolor barcoding technique which involved an epitaxial end-on growth of UCNPs comprising different lanthanide activators on the $NaYF_4$ microrods.[158] In this manner, they fulfilled six kind of multicolor-banded microrods for optical labeling applications.

Apart from basic multicolor outputs, novel energy transfer pathways could be generated through the active-core/active shell interfaces. Chen's group described an interesting type of multicolor emitting $NaGdF_4$:Yb,Tm@$NaGdF_4$:Eu core/shell nanostructures.[159] Under excitation with NIR photons, upward transitions would occur in Tm^{3+} doped core region. Subsequently, energy transfer from the high-lying $^1D_2$ state of Tm^{3+} to ^5L_J state of Eu^{3+} took place. After relaxations to the ^5D_J (J = 0 – 2) states, typical Eu^{3+} emissions were produced. Time-resolved UC spectra revealed the energy transfer pathway apparently. Liu and coworkers further promoted the energy transfer pathway from Tm^{3+} to activators without long-lived intermediate energy levels, including Eu^{3+}, Tb^{3+}, Dy^{3+}, and Sm^{3+}.[34] Such a novel energy transfer pathway is called EMU, which was mentioned in the section of mechanisms of UC emissions. As shown in Fig. 15, four types of luminescent centers are embedded in separated layers. Energy transfer would occur *via* Gd^{3+} ($^6P_{7/2}$ state) through the core/shell

interface. Further coating with an inert $NaYF_4$ shell layer efficiently prevented surface quenching of excitation energy.[160]

5.3.2 luminescence resonance energy transfer (LRET)

Energy transfers from an excited entity (donor) to another entity (acceptor) can take place in two different manners, radiatively and non-radiatively. The radiative energy transfer involves emission of photons from donors and subsequent absorption by acceptor. In contrast, the non-radiative energy transfer refers to simultaneous occurrence of deactivation of donor and excitation of acceptor. Such a unique energy transfer pathway is called "resonant energy transfer (RET)". According to the theory of RET, two key factors determine the efficiency of RET process, overlap between the emission band of donor and absorption band of acceptor, and the spatial distance between the two counterparts.

With narrow and less efficient absorption from 4f-4f transitions, UCNPs are usually employed as donors, while some fluorescent dyes, quantum dots, and noble metals act as the energy acceptors. UC emissions excited by 980 nm can be absorbed by spectrally-matched acceptors. Because of sharp emission profiles, large anti-Stokes shifts, and long luminescence lifetime, UCNPs are in the ascendant as alternative donors in RET studies. The RET process concerning emission from rare earth is usually called "luminescence resonance energy transfer (LRET)". Highly efficient modulation of UC emission can also be engendered through LRET processes.

Biorecognition was demonstrated with LRET between $NaYF_4$:Yb,Er and gold NCs.[161] The green emission of Er^{3+} was tuned subtly with increasing introduction of gold NCs. Zhang and coworkers demonstrated a multicolor emitting UCNPs with LRET.[162] Two frequently used fluorescent dyes, fluorescein
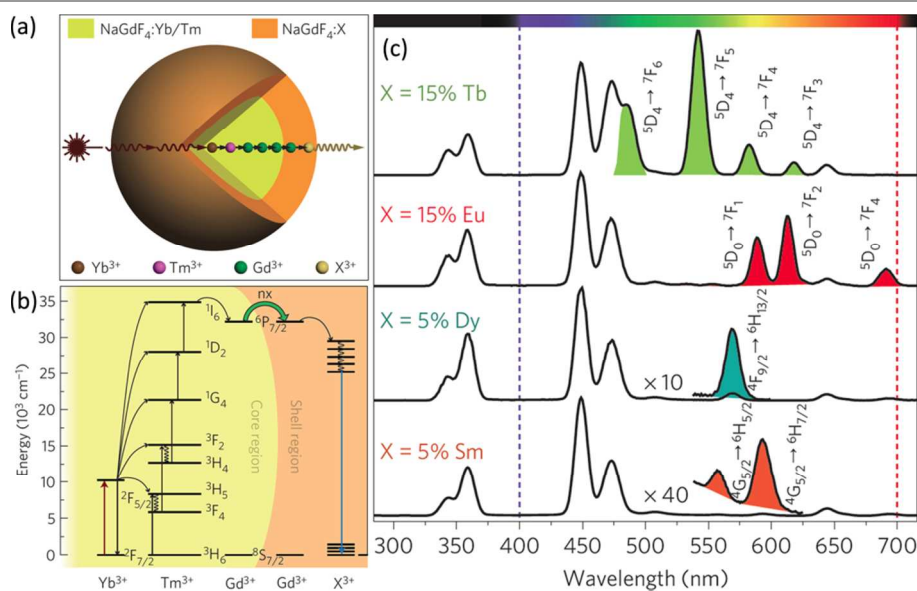
Fig. 15 (a) Schematic design of lanthanide-doped $NaGdF_4$@$NaGdF_4$ core/shell NCs for EMU. (b) Proposed energy transfer mechanisms in the core-shell NC. (c) Emission spectra of the as-prepared $NaGdF_4$@$NaGdF_4$ core/shell NCs doped with different activators. (Modified with permission from ref. 34. Copyright 2011, Nature Publishing Group.)

isothiocyanate (FITC) and tetramethylrhodamine isothiocyanate (TRITC), and quantum dots (QD605) were encapsulated into the silica shell coated outside of NaYF$_4$:Yb,Er/Tm NCs. Reduction of characteristic emission peaks of NaYF$_4$:Yb,Er/Tm NCs and appearance of new emission peaks of FITC, TRITC, and QD605 confirmed the occurrence of LRET processes. We presented another example of LRET between NaYF$_4$:Yb,Er NCs and TRITC.[163] The change in spectral profiles and decay curves revealed LRET from UCNPs to TRITC. Liu *et al.* grafted Rhodamine B (RhB), Rhodamine 6G (Rh6G), and Tide Quencher 1 (TQ1) on the surface of Er^{3+} activated UCNPs, yielding multicolor emissions.[164] Furthermore, they applied the modified UCNPs for multicolor *in vivo* imaging. Gorris *et al.* realized subtly tuning of UC emissions *via* LRET between UCNPs and organic dyes. NaYF$_4$:Yb,Er NCs displayed green and red ($^4F_{9/2} \rightarrow {}^4I_{15/2}$) emissions were encoded by RhB and dye S-0378, respectively.[165] For NaYF$_4$:Yb,Tm NCs, fluorescein and dye NIR-797 were employed to encode the blue ($^1G_4 \rightarrow {}^3H_6$) and NIR ($^3H_4 \rightarrow {}^3H_6$) emissions, respectively (Fig. 16).

As reported, MnO$_2$ nanosheets formed on the surface of UCNPs served as an efficient quencher for UC luminescence.[166] However, the luminescence could be turned on by introducing glutathione that reduced MnO$_2$ into Mn^{2+}. Graphene oxide (GO) materials have been demonstrated as efficient energy acceptors. Li *et al.* assembled ssDNA modified UCNPs with GO *via* strong $\pi - \pi$ stacking effect.[167] As a result, complete quenching of UC emission was observed in the composite. When adenosine triphosphate (ATP) was added, UCNPs were dissociated with GO as ss-DNA was designed as ATP aptamer. Therefore, UC luminescence was recovered. Zhang[168] and Zhao[169] also demonstrated efficient energy transfer from UCNPs to GO related materials lately.

In a fascinating demonstration, V. Mahalingam *et al.* observed interparticle energy transfer (Yb^{3+} → Tm^{3+}, Ho^{3+}) in sub-5 nm Ln^{3+} doped BaLuF$_5$ NCs.[170] Sensitizers (Yb^{3+}) and activators (Tm^{3+}, and Ho^{3+}) were independently doped in BaLuF$_5$ NCs. Recognizable UC emissions could be observed from the mixture of colloidal solutions after an equilibration process. Beyond that, Liu *et al.* also reported the interparticle energy transfer (Gd^{3+} → Gd^{3+}) in the EMU related UCNPs after removal of surface capping ligands.[34]

5.4 Regulating Dynamic Processes

Within an upconverting process, corresponding excitation, radiative emission and non-radiative relaxation processes are possessed of diverse transition rates. Accelerated excitation and emission processes are favorable for overall UC emission intensity, while enhanced rate of non-radiative transition is conducive to weakening of UC emissions. To date, interaction with localized surface plasmon resonances (LSPRs) and ultra-high power excitations have been proved to be effective for modulation of UC dynamic processes.

5.4.1 localized surface plasmon resonance (LSPR) assisted energy transfer

In recent decades, LSPR enhanced fluorescence has been
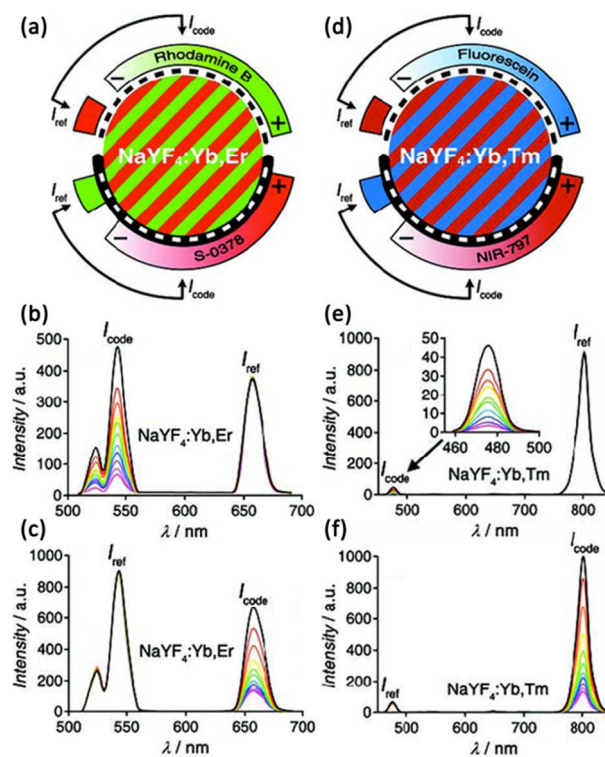
Fig. 16 (a) Different concentrations of either RhB or S-0378 on the surface of NaYF$_4$:Yb,Er UCNPs used to screen off selectively ether green or red emission band to various degrees. Green (b) and red (c) emissions (I_{code}) of NaYF$_4$:Yb,Er UCNPs adjusted in ten increments by increasing the concentration of RhB and S-0378, respectively, while he second band (I_{ref}) remained constant. (d) Fluorescein or NIR-797 screen off the blue or the NIR emission band of NaYF$_4$:Yb,Tm UCNPs. (e, f) Adjusting specifically the blue (e) or the NIR (d) emission (I_{code}) of NaYF$_4$:Yb,Tm UCNPs by either fluorescein or NIR-797 yielded similar results. (Modified with permission from ref. 165. Copyright 2011, Wiley-VCH Verlag GmbH & Co. KGaA.)

extensively studied in organic fluorophores, QDs, as well as UCNPs.[22,171,172] Commonly employed plasmonic materials mainly focus on noble metals like gold and silver. Two possible factors may account for the enhancement effect. For one thing, an amplification of the local incident electromagnetic field leads to an increase of the excitation rate, which arises from the resonant coupling with SPR of noble metals. For another, an increase of the emission rate by surface plasmon coupled emission result in enhanced emission efficiency, which will effectively promote the radiative and non-radiative decay rate. In this case, quenching effects can also be observed due to the significant enhancement in non-radiative decay rate. Coupling with the excitation process takes place when the excitation band of the fluorophore overlaps consistent with the plasmon resonance frequencies, while coupling with the emission process is able to occur in the situation of overlap between the emission band of the fluorophore and the LSPR band of noble metals.

Our group demonstrated noticeable enhancement of UC emission intensity by LSPR for the first time.[173] In our investigation, sub-micron-long Ag nanowires were chosen to provide LSPRs while NaYF$_4$:Yb,Er NCs were employed as UC emission generators. As shown in the optical microscopy image

and corresponding mapping profile from green emission (Fig. 17a, b), the emission intensity of NaYF$_4$:Yb,Er NCs increased sizably where there were Ag nanowires. Spectral results (Fig. 17c) showed that the enhancement factor was *ca.* 2.3 and 3.7 for green ($^2H_{11/2}$, $^4S_{3/2}$ → $^4I_{15/2}$) and red ($^4F_{9/2}$ → $^4I_{15/2}$) emissions, respectively. With the comparison with 8 nm Ag NCs and 10 nm Au NCs, we attributed part of the enhancement to size induced scattering effect.

Duan and coworkers investigated UC spectral profiles from composites of NaYF$_4$:Yb,Tm NCs attached with Au NCs.[174] Specifically, more than 150% increase in emission intensity was observed at 452 nm ($^1D_2$ → $^3F_4$) and 476 nm ($^1G_4$ → $^3H_6$), while an increase of only approximately 50% was detected at 647 nm($^1G_4$ → $^3F_4$). Interestingly, quenching effect was noticed when Au NCs formed as a shell embraced the UCNPs. This enhancement was ascribed to increase of the radiative decay rate and emission efficiency while the quenching was attributed to considerable scattering of excitation irradiation. Later, another work demonstrated an average enhancement factor of 5.1 and a largest enhancement factor of more than 10 in NaYF$_4$:Yb,Er NCs when coupled with gold island films.[175] Increased excitation flux originated from local field enhancement was regarded as the main inducement.

Qin's group demonstrated two orders of magnitude enhancement in Au@NaYF$_4$:Yb,Tm composites compared with counterpart without Au NCs.[176] It is worth noting that five-photon UC emissions located at 290 nm ($^1I_6$ → $^3H_6$) and 345 nm ($^1I_6$ → $^3F_4$) exhibited larger enhancement factor. Prolonged lifetimes of Yb^{3+} and Tm^{3+} excited states suggested that the enhanced UC emissions are induced by plasmon field enhancement of attached Au NCs. Under the same principle, they observed 76 and 47 times enhancement in emissions at ~278 nm ($^6I_{7/2}$ → $^8S_{7/2}$) and 315 nm ($^6P_{5/2}$ → $^8S_{7/2}$) of Gd^{3+}.[177]
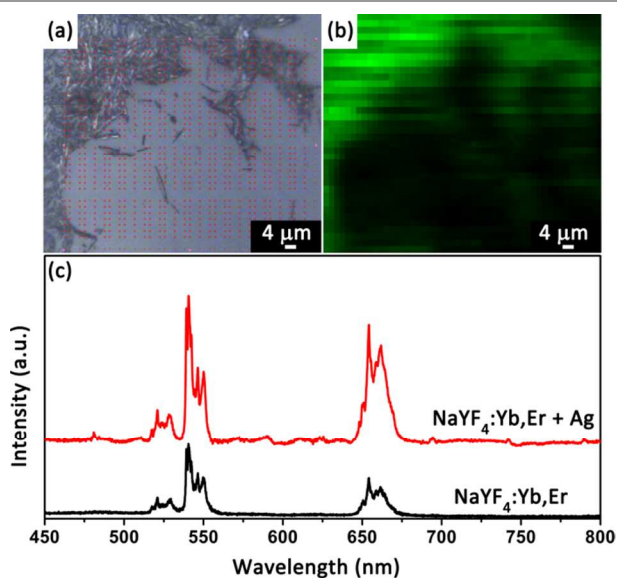
Fig. 17 Optical microscopy image (a), corresponding mapping profile from green emission (b), and UC spectra of NaYF$_4$:Yb,Er NCs and Ag − NaYF$_4$:Yb,Er composites on silicon substrate with the excitation of a 980 nm diode laser (c). Adapted from ref. 173.

This is the first demonstration of emission enhancement of Gd^{3+} *via* energy transfer from co-doped Tm^{3+}: $^3P_2$ (Tm^{3+}) → ^6I_J (Gd^{3+}). Zhang's group adjusted the LSPR peak of composites comprising NaYF$_4$:Yb,Er@SiO$_2$ NCs and Au shells by regulating the thickness of shell layer, ranging from 580 nm to 900 nm.[178] Spectral results showed enhanced emissions only in composite whose LSPR peaks at 900 nm, nearest to the excitation band. The enhanced factor was found to be 2.1, 2.6, and 3.3 for red, green, and violet ($^2H_{9/2}$ → $^4I_{15/2}$) emissions, respectively. Such a result indicated that the excitation flux was increased *via* local field enhancement effect.

The separation distance from the LSPR entity is also studied for NaYF$_4$:Yb,Er@SiO$_2$@Ag.[179] By controlling the shell thickness of the silica spacer, different extent of modulation was found. The optimum UC luminescence enhancement (14.4-fold and 10.8-fold) was observed at a separation distance of 10 nm for Ag NPs with two different sizes (15 and 30 nm). The separation distance dependent emission intensity was ascribed to the competition between enhanced radiative decay rate and energy transfer from UCNPs to non-emissive noble metals. Kagan *et al.* investigated metal-oxide-UCNP tri-layered structure where the thickness of the oxide spacer was precisely varied from 2 to 15 nm.[180] From their study, the optimum separation distance showed strong dependence upon the type of metal NCs, 5 nm for Au NCs and 10 nm for Ag NCs. For structures made with Au NCs, they observed enhancement factors of about 5.2 and 3.5 for the green and red emissions of NaYF$_4$:Yb,Er NCs respectively, and much larger enhancement factors of 30 and 45 with Ag NCs for green and red emissions, respectively. Time-resolved rise and decay time measurements showed that the enhancement arose from amplification of excitation and increase in the radiative rate of emission. In the same principle, they discovered up to 35-fold enhancement in emission intensity from NaYF$_4$:Yb,Er NCs localized in arrays of subwavelength holes in Au films.[181] Schietinger *et al.* investigated assembly of single UCNP and gold NC in a combined confocal and atomic force microscope setup.[182] An overall enhancement factor of 3.8 was reached when they were in close vicinity, 4.8 times enhancement for green emission and 2.7 times enhancement for red emission. Time-resolved characterizations indicated a combined faster excitation and emission rate.

Fine arrays of noble metals have been demonstrated as efficient energy donors. P. S. May *et al.* observed over 3 times enhancement for UC emissions from the patterned gold surface.[183] Approximate 2-fold magnification of the excitation field intensity was demonstrated relative to smooth gold. Recently, the authors reported Au nanopillar arrays enhanced NIR emissions from NaYF$_4$:Yb,Tm NCs with an enhancement factor of ~5.5.[184] Interestingly, they discovered a new peak near 780 nm ($^1G_4$ → $^3H_5$) after combination with Au nanopillar arrays. Recently, Nagpal and coworkers reported plasmon-enhanced resonant energy transfer from Yb^{3+} to Er^{3+} on gold pyramid pattern by at least 6 times.[185] The quenching was also increased ~14 times on the flat metal which pointed to the need

for the careful coupling of the plasmon modes with the desired photophysical processes.

As mentioned, introduction of noble metals can also weaken UC emissions due to the prominent increase in non-radiative decay rate. Li *et al*. developed a facile method to modulate UC emissions from NaYF$_4$:Yb,Er@SiO$_2$ NCs by decoration with Au NCs.[186] With increasing amount of Au NCs attached to the surface of UCNPs, an obvious decrease in emission intensity of Er^{3+} occurred. Moreover, green emission decayed faster than red emission due to the better spectral overlap with the LSPR band of Au NCs.

5.4.2 ultra-high power excitation

In a conventional excitation power dependent UC spectral investigation, saturation of UC processes can be frequently observed at high excitation power density. That is, UC emission intensity would not increase continuously with elevated excitation power density. Under 980 nm excitation, we have noticed saturation effect in α-NaYF$_4$:Yb,Er and β-NaYF$_4$:Yb,Er NCs (Yb: 20%, Er: 2%) after the excitation power density reached 1.3 W cm^{-2}.[61] Suggested by Suyver *et al* in 2005, such a saturation effect proved that the present UC processes were ETU types involving energy transfer from Yb^{3+} to Er^{3+}.[64] However, UC properties became entirely different in several recent studies, which were conducted under ultra-high excitation power densities.

Wu *et al*. studied the photostability of β-NaYF$_4$:Yb,Er NCs by monitoring the luminescent image of individual UCNPs with a sample-scanning confocal optical microscope.[187] With a tightly focused excitation of a 980 nm CW laser, the branch ratio of red ($^4F_{9/2} \rightarrow {}^4I_{15/2}$) to green ($^2H_{11/2}$, $^4S_{3/2} \rightarrow {}^4I_{15/2}$) emission increased sizably under high power excitation. *I-P* curve uncovered the reason that red emissions enhanced faster than green emission as pump power density increased.

Last year, Jin *et al*. demonstrated that intensive irradiation (2.5×10^6 W cm^{-2}) can alleviate concentration quenching in UC luminescence, and a much higher doping concentration of 8% Tm^{3+} in NaYF$_4$ was addressed.[188] Former studies showed that considerable cross-relaxation, $^1G_4 + {}^3H_6 \rightarrow {}^3H_4 + {}^3H_5$, played the key role in luminescence quenching under low power excitations.[62] By comparison, an ultra-high laser beam can assist the upward transition from the $^3H_4$ states. Respective population ratios of $^1D_2$ and $^1G_4$ to $^3H_4$ with various Tm^{3+} content and irradiance ($1 \times 10^4 - 2.5 \times 10^6$ W cm^{-2}) revealed the hypothesis. Increasing excitation irradiance from 1.6×10^6 W cm^{-2} to 2.5×10^6 W cm^{-2} enhanced the overall UC emission intensity by factors of 5.6, 7.1, and 1105 for 0.5%, 4%, and 8% Tm^{3+}, respectively.

Lately, Schuck and coworkers reported the similar phenomenon in heavily Er^{3+}-doped (20%) UNCPs under ultra-high excitation power density.[189] As shown in Fig. 18, the emission from NaYF$_4$:20%Yb,20%Er NCs vanished at lower powers, while conventionally used 2% Er^{3+} doped counterpart exhibited much brighter emission. As excitation power increased, the conventional UCNPs saturated in brightness while high-Er^{3+} doped UCNPs became visible and continued to
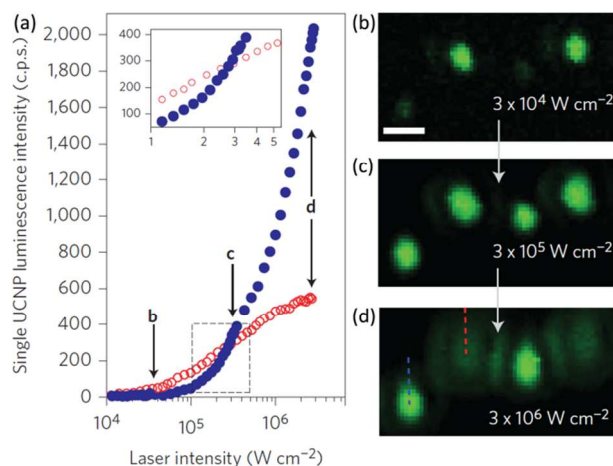
Fig. 18 Luminescence intensity of single 8 nm UCNPs with 20% (blue circles) and 2% (red circles) Er^{3+}, each with 20% Yb^{3+}, plotted as function of excitation intensity. Inset: zoom-in of the luminescence intensity cross-over region for UCNPs with the two different emitter concentrations. (b – d) Confocal luminescence images taken at points shown in (a) of a single UCNPs containing a mixture of 2% and 20% Er^{3+}. The images were collected at increasing excitation intensities. Dashed lines indicate regions for which luminescence intensity was collected for data in (a). Scale bar, 1 μm. (Modified with permission from ref. 189. Copyright 2014, Nature Publishing Group.)

increase in brightness, surpassing the conventional UCNPs. Over 3×10^5 W cm^{-2}, 20% Er^{3+} doped UCNPs became brighter suddenly than the 2% Er^{3+} counterpart. Moreover, they found that $^2F_{5/2}$ excited state of Yb^{3+} had its population approach 70% of the overall Yb^{3+} concentration, well into saturation regime. The authors argued that the fundamental bottleneck of Er^{3+} emitters should be attributed to the significantly slower radiative relaxation rates for parity-forbidden 4f-4f transitions than photon absorption rates.

6 Energy Transfer Triggered Novel Excitations

Conventional ETU based UCNPs, which are sensitized by Yb^{3+} ions, exhibit narrowband absorption located at 980 nm ($^2F_{7/2} \rightarrow {}^2F_{5/2}$). Actually, other NIR wavelengths have been tested and verified to expand the selection of excitation wavelengths. He and coworkers demonstrated a series of 915 nm excited NaYbF$_4$:Ln (Ln = Er, Tm, Ho) NCs.[190] Realization of 915 nm excitation should be attributed to the shoulder absorption peak around 915 nm. And it generated similar UC emissions with that of 980 nm irradiation. Prasad's group described a type of 1490 nm excited LiYF$_4$:Er NCs.[191] Without sensitization from Yb^{3+}, UC emissions are yielded by less efficient ESA upward transitions, accompanied with multiphoton cross-relaxations within Er^{3+} ions. As a result, green ($^2H_{11/2}$, $^4S_{3/2} \rightarrow {}^4I_{15/2}$) and red ($^4F_{9/2} \rightarrow {}^4I_{15/2}$) emissions are demonstrated as three-photon UC transitions.

Despite of these accomplishments, limited excitation selections still hinder the flexibility of further applications. To solve the pending questions, researchers have developed novel excitations *via* energy transfer from organic antenna or lanthanides.

Hummelen *et al.* provided a much-needed solution that allowed for more flexibility across a broad range of excitation wavelengths.[192] In their study, carboxyl-containing chains were grafted to commercial IR-780 cyanine dye molecules to render coordination with Ln^{3+} on the surface of UCNPs. The modified antenna dyes trapped NIR photons (650 – 850nm) and then transferred the energy to Yb^{3+} embedded in the matrix *via* Förster resonance energy transfer (FRET). Finally, the energy was extracted by Er^{3+}, generating visible UC emissions. Spectral results exhibited a 3300-fold enhancement under excitation with 800 nm excitation compared with that under 980 nm irradiation. An obvious broad band arose in the range of 740 – 850 nm in the excitation spectra, corresponding to the squared absorption of IR-806.

As alternatives, our group presented a novel route to shift the excitation band within the NIR range (Fig. 19).[193] The newly constructed UCNPs were directly sensitized by Nd^{3+} ions. With the energy transfer process, $^4F_{3/2}$ (Nd^{3+}) $\rightarrow$ $^2F_{5/2}$ (Yb^{3+}), electrons were populated on the exited state of Yb^{3+} ($^2F_{5/2}$) under the excitation of Nd^{3+} at 800 nm. Subsequently, Er^{3+} trapped the energy and yielded UC emissions. To avoid mutual quenching between Nd^{3+} and Er^{3+} ions, core/shell structured $NaGdF_4:Yb,Er@NaGdF_4:Nd,Yb$ were fabricated. Benefiting from the larger absorption cross-section of Nd^{3+} (5.8×10^{-20} cm^{-1}) around 800 nm, a similar excitation efficiency to that of 980 nm was demonstrated. Moreover, the heating effect induced by 980 nm irradiation was considerably minimized due to the much weaker water absorption at ~800 nm.

Han and coworkers demonstrated cascade sensitization of UCNPs at 800 nm.[194] Precisely defined amount of Nd^{3+} was tri-doped with Yb^{3+} and activators in the same layer. Liu's group performed the mechanistic investigation into tri-doped UCNPs with Nd^{3+}-sensitization.[195] Wang *et al.* realized the energy transfer management in core/shell/shell NCs under 808 nm excitation.[196] Besides Er^{3+}, Tm^{3+}, and Ho^{3+}, the authors observed UC emissions from Eu^{3+}, Tb^{3+}, and Dy^{3+} under 808 nm excitation. To further prevent the EBT process: $^4I_{11/2}$ (Er^{3+}) + $^4I_{9/2}$ (Nd^{3+}) $\rightarrow ^4I_{13/2}$ (Er^{3+}) + $^4I_{13/2}$ (Nd^{3+}) and $^4I_{13/2}$ (Er^{3+}) + $^4I_{9/2}$ (Nd^{3+}) $\rightarrow ^4I_{15/2}$ (Er^{3+}) + $^4I_{15/2}$ (Nd^{3+}), a Yb^{3+}-doped $NaYF_4$ layer was inserted between the Er^{3+} and Nd^{3+} containing layer.[197] Zhang *et al.* synthesized the Nd^{3+} sensitized up/down converting dual-mode NCs for efficient bioimaging excited at 800 nm.[198] Such a successful shift from absorption of water molecules renders the Nd^{3+} sensitized UCNPs much more applicable for *in vivo* applications.

7 Conclusions and Perspective

In this review, we described energy transfers and recent development in modulation of energy transfer pathways relevant in Ln^{3+} based UC emissions. Efforts devoted to manipulating energy transfer distance, introducing extraneous energy levels, incorporating energy extractors or passivators, and regulating UC dynamic processes are demonstrated as valuable contributions. Purposeful control of energy transfer pathway is able to generate precise-tuning of UC emissions.
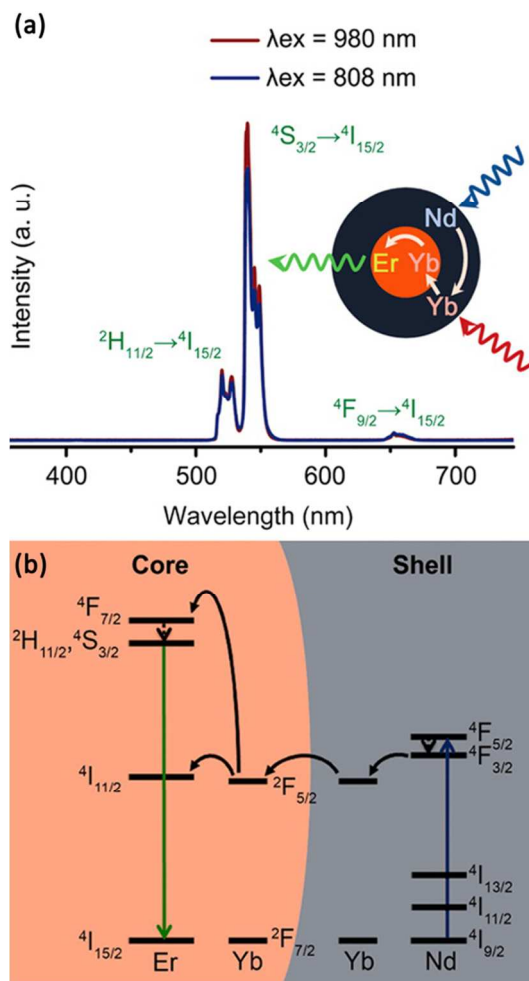
Fig. 19 (a) UC emission spectra of $NaGdF_4:Yb,Er@NaGdF_4:Nd,Yb$ NCs under 980 nm and 808 nm excitations. Inset is the schematic design of core/shell structured UCNPs. (b) Energy transfer pathways $Nd^{3+} \rightarrow Yb^{3+} \rightarrow Er^{3+}$ in the core/shell structured NCs under 808 nm excitation. (Modified with permission from ref. 193. Copyright 2013 American Chemical Society.)

Furthermore, we introduced the emerging progresses in excitation selection. With energy transfer from organic antenna and alternative lanthanide sensitizer (Nd^{3+}) to lanthanides, the excitation band shifted successfully, yielding similar excitation efficiency and minimized heating effect induced by original irradiation. In general, introduction of the epitaxial shell is a more convenient and flexible way to modulate the UC energy transfer pathways. Thus exploring novel core/shell nanostructures is quite meaningful to generate desired UC emissions and also excitations.

Due to the unique NIR excitation, large anti-Stokes shift, sharp-band emission, excellent photostability, remarkable penetration depth, and low toxicity, UCNPs exhibit exceedingly promising potentials in bioimaging and theranostic studies. To date, various *in vitro* and *in vivo* models have been selected to investigate the imaging values of UCNPs, including cells,[199] bacteria,[200] elegans,[201,202] mice,[203,204] and rabbits[205]. Besides the single-mode of imaging, NIR triggered UCNPs have been combined with X-ray computed tomography (CT),[206] magnetic

resonance imaging (MRI),[207] and single-photon emission computed tomography (SPECT)[208] to provide synergistic effects. Moreover, UCNPs have been employed to serve as the carrier to conduct drug delivery *in vivo*.[219,210] Owing to the spatial (remote control) and temporal (on demand) advantages, light is widely used as external stimuli to manipulate chemical reactions.[211–213] Conventionally used UV and visible lights exhibit several drawbacks on account of the inherent high photon energy, such as potential material decomposition and limited penetration depth. In comparison, NIR light is more fascinating due to its lower photon energy. Profiting from upconverting ability, UCNPs are employed to upconvert NIR light to short-wavelength photons to direct photochemical reactions. To date, various photochemical reactions have been demonstrated and highlighted the elegancy of UCNPs as an excellent energy transducers, including photoswitch,[214,215] photorelease,[216,217] photoisomerization,[218,219] photodynamic therapy,[220,221] and sensing and detection[222,223].

Despite of these achievements, further unambiguous attentions should be paid to develop novel UC energy transfers with high efficiency toward potential applications. Besides current UC emission modulations that mainly centered at Er^{3+} and Tm^{3+}, skillful mastery of UC energy transfer pathways in other Ln^{3+} is also needful, such as Pr^{3+}, Sm^{3+}, and so forth. Only in this way, wavelength-tunable UC emissions could be obtained in level-fixed Ln^{3+}. Certain meaningful modulation manners should be kept on exploring, for example, local crystal field tailoring, mutual interaction with Ln^{3+} and transition metal ions, and heavily activator-doped UCNPs under ultra-high pump power excitation. It is worth noting that the short-wavelength infrared emissions, which are arisen from the relaxation processes of upward transitions in Er^{3+}, Ho^{3+}, Tm^{3+}, and Pr^{3+}, are also of high research values. Compared with the visible and NIR emissions, the short-wavelength infrared emissions possess remarkable penetration depth capability.[224]

To date, only one type of NIR antenna has rendered UC go to broadband excitation. More investigations should be focused on the enhancement of UC efficiency *via* energy transfer from organic antennas or quantum dots which are with larger absorption cross-section. Emergence of Nd^{3+} sensitized UC emission offers significant chance for biological applications. Yb^{3+} sensitized UCNPs for *in vitro* and *in vivo* investigations are expected to be replaced gradually by Nd^{3+} sensitized counterparts due to their enhanced biocompatibility. As such, potential energy transfer based photochemical applications would be vastly boomed on account of the m choice of UC excitations. We believe that with well-designed energy transfers, investigations of UCNPs would continue to be a hotspot in interdisciplinary field.

Acknowledgements

Notes and references

Beijing National Laboratory for Molecular Sciences, State Key Laboratory of Rare Earth Materials Chemistry and Applications, PKU-HKU Joint Laboratory in Rare Earth Materials and Bioinorganic Chemistry, Peking University, Beijing 100871, China. Fax: +86-10-62754179; Tel: +86-10-62754179; Email: sun@pku.edu.cn, yan@pku.edu.cn.

1   F. Auzel, *Chem. Rev.*, 2004, **104**, 139–173.
2   J.-C. G. Bünzli, S. Comby, A.-S. Chauvin and C. D. B. Vandevyver, *J. Rare Earth*, 2007, **25**, 257–274.
3   J. Shen, L. D. Sun and C. H. Yan, *Dalton Trans.*, 2008, 5687–5697.
4   A. de B.-Dias, *Dalton Trans.*, 2007, 2229 – 2241.
5   B. M. van de Ende, L. Aarts and A. Meijerink, *Phys. Chem. Chem. Phys.*, 2009, **11**, 11081–11095.
6   S. V. Eliseeva and J.-C. G. Bünzli, *Chem. Soc. Rev.*, 2010, **39**, 189–227.
7   D. K. Chatterjee, M. K. Gnanasammandhan and Y. Zhang, *Small*, 2010, **6**, 2781–2795.
8   C. Zhang, L. D. Sun, Y. W. Zhang and C. H. Yan, *J. Rare Earth*, 2010, **28**, 807–819.
9   X. Y. Huang, S. Y. Han, W. Huang and X. G. Liu, *Chem. Soc. Rev.*, 2013, **42**, 173–201.
10 Y. Q. Liu, J. B. Zhao, R. Zhang, Y. J. Liu, D. M. Liu, E. M. Goldys, X. S. Yang, P. Xi, A. Sunna, J. Lu, Y. Shi, R. C. Leif, Y. J. Huo, J. Shen, J. A. Piper, J. P. Robinson and D. Y. Jin, *Nat. Photonics*, 2014, **8**, 32–36.
11 S. L. Gai, C. X. Li, P. P. Yang and J. Lin, *Chem. Rev.*, 2014, **114**, 2343–2389.
12 N. Bloembergen, *Phys. Rev. Lett.*, 1959, **2**, 84–85.
13 J. F. Suyver, A. Aebischer, D. Biner, P. Gerner, J. Grimm, S. Heer, K. W. Krämer, C. Reinhard and H. U. Güdel, *Opt. Mater.* 2005, **27**, 1111–1130.
14 F. Wang and X. G. Liu, *Chem. Soc. Rev.*, 2009, **38**, 976–989.
15 M. Haase and H. Schäfer, *Angew. Chem. Int. Ed.* 2011, **50**, 5808–5829.
16 G. F. Wang, Q. Peng, and Y. D. Li, *Acc. Chem. Res.*, 2011, **44**, 322–332.
17 Z. J. Gu, L. Yan, S. J. Li, Z. F. Cai and Y. L. Zhao, *Adv. Mater.*, 2013, **25**, 3758–3779.
18 X. M. Li, F. Zhang and D. Y. Zhao, *Nano Today*, 2013, **8**, 643–676.
19 W Feng, C. M. Han and F. Y. Li, *Adv. Mater.*, 2013, **25**, 5287–5303.
20 P. Y. Qiu, N. Zhou, H. Y. Chen, C. L. Zhang, G. Gao and D. X. Cui, *Nanoscale*, 2013, **5**, 11512–11525.
21 G. Y. Chen, H. L. Qiu, P. N. Prasad and X. Y. Chen, *Chem. Rev.*, 2014, **114**, 5161–5214.
22 H. Dong, L. D. Sun and C. H. Yan, *Nanoscale*, 2013, **5**, 5703–5714.
23 F. Wang and X. G. Liu, *Acc. Chem. Res.*, 2014, **47**, 1378–1385.
24 F. Wang, D. Banerjee, Y. S. Liu, X. Y. Chen and X. G. Liu, *Analyst*, 2010, **135**, 1839–1854.
25 J. Zhou, Z. Liu and F. Y. Li, *Chem. Soc. Rev.,* 2012, **41**, 1323–1349.
26 L. D. Sun, Y. F. Wang and C. H. Yan, *Acc. Chem. Res.*, 2014, **47**, 1001–1009.
27 J. S. Chivian, W. E. Case and D. D. Eden, *Appl. Phys. Lett.*, 1979, **35**, 124–125.
28 H. Deng, S. H. Yang, S. Xiao, H. M. Gong and Q. Q. Wang, *J. Am. Chem. Soc.*, 2008, **130**, 2032–2040.

29   W. Strek, P. Deren and A. Bednarkiewicz, *J. Lumin.*, 2000, **87–89**, 999–1001.

30   Y. Arai, T. Yamashidta, T. Suzuki and Y. Ohishi, *J. Appl. Phys.* 2009, **105**, 083105.

31   I. Hernández, N. Pathumakanthar, P. B. Wyatt and W. P. Gillin, *Adv. Mater.*, 2010, **22**, 5356–5360.

32   M. L. Debasu, D. Ananias, S. L. C. Pinho, C. F. G. C. Geraldes, L. D. Carlos and J. Rocha, *Nanoscale*, 2012, **4**, 5154–5162.

33   K. Prorok, A. Gnach, A. Bednarkiewicz and W. Strek, *J. Lumin*, 2013, **140**, 103–109.

34   F. Wang, R. R. Deng, J. Wang, Q. X. Wang, Y. Han, H. M. Zhu, X. Y. Chen and X. G. Liu, *Nat. Mater.*, 2011, **10**, 968–973.

35   F. Auzel, *Proc. IEEE* 1973, **61**, 758–786.

36   F. Auzel and D. Pecile, *J. Lumin.*, 1973, **8**, 32–43.

37   F. Auzel, D. Pecile and D. Morin, *J. Eletrochem. Soc.*, 1975, **122**, 101–107.

38   F. Auzel and D. Pecile, *J. Lumin.*, 1976, **11**, 321–330.

39   M. A. Chamarro and R. Cases, *J. Lumin.*, 1988, **42**, 267–274.

40   J. A. Capobianco, F. Vetrone and J. C. Boyer, *J. Phys. Chem. B*, 2002, **106**, 1181–1187.

41   F. van de Rijke, H. Zijlmans, S. Li, T. Vail, A. K. Raap, R. S. Niedbala and H. J. Tanke, *Nat. Biotechnol.*, 2001, **19**, 273–276.

42   S. Heer, O. Lehmann, M. Haase and H. U. Güdel, *Angew. Chem. Int. Ed.*, 2003, **42**, 3179–3182.

43   S. Heer, K. Kömpe, H. U. Güdel and M. Haase, *Adv. Mater.*, 2004, **16**, 2102–2105.

44   G. F. Wang, Q. Peng and Y. D. Li, *J. Am. Chem. Soc.*, 2009, **131**, 14200–14201.

45   D. Q. Chen, L. Lei, R. Zhang, A. P. Yang, J. Xu and Y. S. Wang, *Chem. Commun.*, 2012, **48**, 10630–10632.

46   N. Menyuk, K. Dwight and J. W. Pierce, *Appl. Phys. Lett.*, 1972, **21**, 159–161.

47   J. F. Suyver, J. Grimm, K. W. Krämer and H. U. Güdel, *J. Lumin.*, 2005, **114**, 53–59.

48   K. W. Krämer, D. Biner, G. Frei, H. U. Güdel, M. P. Hehlen and S. T. Lüthi, *Chem. Mater.*, 2004, **16**, 1244–1251.

49   X. S. Wang, J. Song, H. Y. Sun, Z. Z. Xu and J. R. Qiu, *Opt. Express*, 2007, **15**, 1384–1389.

50   P. V. Ramakrishna, S. V. N. Pammi and K. Samatha, *Solid State Commun.*, 2013, **155**, 21–24.

51   R. Balda, J. Fernánez, A. Mendioroz, M. Voda and M. Al-Saleh, *Phys. Rev. B*, 2003, **68**, 165101.

52   R. Naccache, F. Vetrone, A. Speghini, M. Bettinelli and J. A. Capobianco, *J. Phys. Chem. C*, 2008, **112**, 7750–7756.

53   X. F. Wang, X. H. Yan ad C. X. Kan, *J. Lumin.*, 2011, **131**, 2325–2329.

54   C. R. Li, S. F. Li, B. Dong, J. C. Sun, X. F. Bao and X. N. Fan, *Chin. Phys. B*, 2012, **21**, 097803.

55   Y. Dwivedi and S. B. Rai, *Opt. Mater.*, 2009, **31**, 1472–1477.

56   R. Martín-Rodríguez, R. Valiente, S. Polizzi, M. Bettinelli, A. Speghini and F. Piccinelli, *J. Phys. Chem. C*, 2009, **113**, 12195–12200.

57   E. Nakazawa and S. Shionoya, *Phys. Rev. Lett.*, 1970, **25**, 1710–1712.

58   T. Jiang, Y. Liu, S. S. Liu, N. Liu and W. P. Qin, *J. Alloys Compd.*, 2012, **377**, 81–87.

59   G.-S. Yi and G.-M.Chow, *J. Mater. Chem.*, 2005, **15**, 4460–4464.

60   M. M. Xing, W. H. Cao, H. Y. Zhong, Y. H. Zhang, X. X. Luo, Y. Fu, W. Feng, T. Pang and X. F. Yang, *J. Alloys Compd.*, 2011, **509**, 5725–5730.

61   H. X. Mai, Y. W. Zhang, L. D. Sun and C. H. Yan, *J. Phys. Chem. C*, 2007, **111**, 13721–13729.

62   A. X. Yin, Y. W. Zhang, L. D. Sun and C. H. Yan, *Nanoscale*, 2010, **2**, 953–959.

63   M. Pollnau, D. R. Gamelin, S. R. Lüthi, H. U. Güdel and M. P. Hehlen, *Phys. Rev. B*, 2000, **61**, 3337–3346.

64   J. F. Suyver, A. Aebischer, S. García-Revilla, P. Gerner and H. U. Güdel, *Phys. Rev. B*, 2005, **71**, 125123.

65   A. M. Pires, S. Heer, H. U. Güdel and O. A. Serra, *J. Fluoresc.*, 2006, **16**, 461–468.

66   V. Singh, V. K. Rai and M. Haase, *J. Appl. Phys.*, 2012, **112**, 06315.

67   V. Singh, V. K. Rai, K. Al-Shamery, M. Haase and S. H. Kim, *Appl. Phys., A* 2013, **113**, 747–753.

68   F. Vetrone, J.-C. Boyer and J. A. Capobianco, *J. Appl. Phys.*, 2004, **96**, 661–667.

69   J. W. Zhao, Y. J. Sun, X. G. Kong, L. J. Tian, Y. Wang, L. P. Tu, J. L. Zhao and H. Zhang, *J. Phys. Chem. B*, 2008, **112**, 15666–15672.

70   F. Wang and X. G. Liu, *J. Am. Chem. Soc.*, 2008, **130**, 5642–5643.

71   Z. G. Xia, J. Li, Y. Luo and L. B. Liao, *J. Am. Ceram. Soc.*, 2012, **95**, 3229–3234.

72   X. H. Chuai, F. X. Yin, Z. Y. Liu, F. Shi, J. S. Wang, L. L. Wang, K. Z. Zheng, C. F. He and W. P. Qin, *Mater. Res. Bull.*, 2013, **48**, 2361–2364.

73   G. Y. Chen, T. Y. Ohulchanskyy, R. Kumar, H. Ågren and P. N. Prasad, *ACS NANO*, 2010, **4**, 3163–3168.

74   J. Shen, G. Y. Chen, T. Y. Ohulchanskyy, S. J. Kesseli, S.Buchholz, Z. P. Li, P. N. Prasad and G. Han, *Small*, 2013, **9**, 3213–3217.

75   X. S. Zhai, S. S. Li, Y. L. Zhang, G. S. Qin and W. P. Qin, *J. Mater. Chem. C*, 2014, **2**, 2037–2044.

76   H. L. Qiu, G. Y. Chen, R. W. Fan, L. M. Yang, C. Liu, S. W. Hao, M. J. Sailor, H. Ågren, C. H. Yang and P. N. Prasad, *Nanoscale*, 2014, **6**, 753–757.

77   D. T. Tu, Y. S. Liu, H. M. Zhu, R. F. Li, L. Q. Liu and X. Y. Chen, *Angew. Chem. Int. Ed.*, 2013, **125**, 1166–1171.

78   T. Soukka, K. Kuningas, T. Rantanen, V. Haaslahti and T. Lövgren, *J. Fluoresc.*, 2005, **15**, 513–528.

79   Y. P. Du, Y. W. Zhang, Z. G. Yan, L. D. Sun, S. Gao and C. H. Yan, *Chem.–Asian J.*, 2007, **2**, 965–974.

80   Y. P. Du, Y. W. Zhang, L. D. Sun and C. H. Yan, *Dalton Trans.* 2009, 8574–8581.

81   G. S, Yi, Y. F. Peng and Z. Q. Gao, *Chem. Mater.*, 2011, **23**, 2729–2734.

82   X. Teng, Y. H. Zhu, W. Wei, S. C. Wang, J. F. Huang, R. Naccache, W. B. Wu, A. I. Y. Tok, Y. Han, Q. C. Zhang, Q. L. Fan, W. Huang, J. A. Capobianco and L. Huang, *J. Am. Chem. Soc.*, 2012, **134**, 8340−8343.

83   Y. J. Ding, X. Teng, H. Zhu, L. L. Wang, W. B. Pei, J. J. Zhu, L. Huang and W. Huang, *Nanoscale*, 2013, **5**, 11928−11932.

84   B. L. An, L. H. Ma, J. H. Fang, Y. Q. Wang and J. Q. Xu, *RSC Adv.*, 2013, **3**, 19909–19912.

85   V. Mahalingam, C. Hazra, R. Naccache, R. Vetrone and J. A. Capobianco, *J. Mater. Chem. C*, 2013, **1**, 6536–6540.

86 S. Sarkar, A. Dash and V. Mahalingam, *Chem.–Asian J.* 2014, **9**, 447–451.

87 J. Wang, F. Wang, J. Xu, Y. Wang, Y. S. Liu, X. Y. Chen , H. Y. Chen and X. G. Liu, *C. R. Chim.*, 2010, **13**, 731–736.

88 P. Huang, W. Zheng, S. Y. Zhou, D. T. Tu, Z. Chen, H. M. Zhu, R. F. Li, E. Ma, M. D. Huang and X. Y. Chen, *Angew. Chem. Int. Ed.*, 2014, **53**, 1252–1257.

89 J. Wang, R. R. Deng, M. A. MacDonald, B. Chen, J. K. Yuan, F. Wang, D. Z. Chi, T. S. A. Hor, P. Zhang, G. K. Liu, Y. Han and X. G. Liu, *Nat. Mater.*, 2014, **13**, 157–162.

90 V. Mahalingam, F. Vetrone, R. Naccache, A. Speghini and J. A, Capobianco, *Adv. Mater.*, 2009, **21**, 4025–4028.

91 F. Shi and Y. Zhao, *J. Mater. Chem. C*, 2014, **2**, 2198–2203.

92 H. X. Mai, Y. W. Zhang, R. Si, Z. G. Yan, L. D. Sun, L. P. You and C. H. Yan, *J. Am. Chem. Soc.*, 2006, **128**, 6426−6436.

93 G. Y. Chen, H. C. Liu, H. J. Liang, G. Somesfalean and Z. G. Zhang, *J. Phys. Chem. C*, 2008**, 112**, 12030–12036.

94 H. Q. Wang and T. Nann, *ACS NANO*, 2009, **3**, 3804–3808.

95 L. Jiang, S. Xiao, X. Yang, J. Ding and K. Dong, *Appl. Phys. B*, 2012, **107**, 477–481.

96 X. Q. Chen, Z. K. Liu, Q. Sun, M. Ye and F. P. Wang, *Opt. Commun.*, 2011, **284**, 2046–2049.

97 K. Mishra, S. K. Singh, A. K. Singh and S. B. Rai, *Mater. Res. Bull.*, 2013, **48**, 4307–4313.

98 Q. Cheng, J. H. Sui and W. Cai, Nanoscale, *Mater. Res. Bull.*, 2013, **48**, 2361–2364.

99 W. Y. Yin, L. N. Zhao, L. J. Zhou, Z. J. Gu, X. X. Liu, G. Tian, S. Jin, L. Yan, W. L. Ren, G. M. Xing and Y. L. Zhao, *Chem.–Eur. J.* 2012, **18**, 9239–9245.

100 H. J. Liang, G. Y. Chen, H. C. Liu and Z. G. Zhang, *J. Lumin.*, 2009, **129**, 197–202.

101 G. Y. Chen, H. C. Liu, G. Somesfalean, Y. Q. Sheng, H. J. Liang, Z. G. Zhang, Q. Sun and F. P. Wang, *Appl. Phys. Lett.* 2008, **92**, 113114.

102 Y. F. Bai, K. Yang, Y. X. Wang, X. R. Zhang and Y. L. Song, *Opt. Commun.*, 2008, **281**, 2930–2932.

103 Y. F. Bai, Y. X. Wang, K. Yang, X. R. Zhang, G. Y. Peng, Y. L. Song, Z. Y. Pan, C. H. Wang, *J. Phys. Chem. C*, 2008**, 112**, 12259–12263.

104 Q. Sun, H. Zhao, X. Q. Chen, F. P. Wang, W. Cai and Z. H. Jiang, *Mater. Chem. Phys.*, 2010, **123**, 806–810.

105 Y. F. Bai, Y. X. Wang, G. Y. Peng, K. Yang, X. R. Zhang and Y. L. Song, *J. Alloys Compd.* 2009, **478**, 678–678.

106 P. Ramasamy, P. Chandra, S. W. Rhee and J. Kim, *Nanoscale*, 2013, **5**, 8711–8717.

107 Y. Li, G. F. Wang, K. Pan, N. Y. Fan, S. Liu and L. Feng, *RSC Adv.*, 2013, **3**, 1683–1686.

108 V. Singh, V. K. Rai, I.-J. Lee, I. Ledoux-Rak, K. Al-Shamery, J. Nordmann and M. Haase, *Appl. Phys. B*, 2012, **106**, 223–22.

109 H. Yu, W. B. Cao, Q. M. Huang, E. Ma, X. Q. Zhang and J. C. Yu, *J. Solid State Chem.*, 2013, **207**, 170–177.

110 J. H. Hao, Y. Zhang and X. H. Wei, *Angew. Chem. Int. Ed.* 2011, **50**, 6876–6880.

111 M. Wang, C. C. Mi, Y. X. Zhang, J. L. Liu, F. Li, C. B. Mao and S. K. Xu, *J. Phys. Chem. C*, 2009**, 113**, 19021–19027.

112 C. M. Zhang, P. A. Ma, C. X. Li, G. G. Li, S. S. Huang, D. M. Yang, M. M. Shang, X. J. Kang and J. Lin, *J. Mater. Chem.*, 2011, **21**, 717–723.

113 Y. Zhang and J. H. Hao, *J. Appl. Phys.*, 2013, **113**, 184112.

114 H. K. Dan, D. C. Zhou, R. F. Wang, T. M. Hau, Q. Jiao, Z. W. Yang, Z. G. Song, X. Yu and J. B. Qiu, *J. Non-Cryst. Solids*, 2013, **378**, 181–185.

115 L. L. Wang, X. J. Xue, H. Chen, D. Zhao and W. P. Qin, *Chem. Phys. Lett.*, 2010, **485**, 183–186.

116 A. S. Gouveia-Neto, L. A. Bueno, R. F. do Nascimento, E. A. de Silva, Jr. and E. B. da Costa, *Appl. Phys. Lett.*, 2007, **91**, 091114.

117 L. L. Xing, X. H. Wu, R. Wang, W. Xu and Y. N. Qian, *Opt. Lett.*, 2012, **37**, 3537–3539.

118 L. L. Xing, Y. L. Xu, R. Wang, and W. Xu, *Opt. Lett.*, 2013, **38**, 2535–2537.

119 G. Y. Chen, H. C. Liu, G. Somesfalean, H. J. Liang and Z. G. Zhang, *Nanotechenol.*, 2009, **20**, 385704.

120 G. F. Wang, Q. Peng and Y. D. Li, *Chem.–Eur. J.* 2010, **16**, 4923–4931.

121 L. J. Huang, L. L. Wang, X. J. Xue, D. Zhao, G. S. Qin and W. P. Qin, J. Nanosci. *Nanotechnol.*, 2011, **11**, 9498–9501.

122 E. M. Chan, G. Han, J. D. Goldberg, D. J. Gargas, A. D. Ostrowski, P. J. Schuck, B. E. Cohen and D. J. Milliron, *Nano Lett.* 2012, **12**, 3839−3845.

123 E. M. Chan, D. J. Gargas, P. J. Schuck and D. J. Milliron, *J. Phys. Chem. B*, 2012, **116**, 10561−1057.

124 O. S. Wenger, D. R. Gamelin, D. R. Gamelin and H. U. Güdel, *J. Am. Chem. Soc.*, 2000, **122**, 7408−7409.

125 D. R. Gamelin and H. U. Güdel, *J. Am. Chem. Soc.*, 1998, **120**, 12143 −12144.

126 D. R. Gamelin and H. U. Güdel, *Inorg. Chem.*, 1999**, 38**, 5154−5164.

127 J. H. Zeng, T. Xie, Z. H. Li and Y. D. Li, *Cryst. Growth Des.*, 2007, **7**, 2774−2777.

128 M. Y. Xie, X. N. Peng, X. F. Fu, J. J. Zhang, G. L. Li and X. F. Yu, *Scripta Mater.*, 2009, **60**, 190−193.

129 J. Wang, F. Wang, C. Wang, Z. Liu and X. G. Liu, *Angew. Chem. Int. Ed.*, 2011, **50**, 10369−10372.

130 Y. Zhang, J. D. Lin, V. Vijayaragavan, K. K. Bhakoo and T. T. Y. Tan, *Chem. Commun.*, 2012, **48**, 10322–10324.

131 G. Tian, Z. J. Gu, L. J. Zhou, W. Y. Yin, X. X. Liu, L. Yan, S. Jin, W. L. Ren, G. M. Xing, S. J. Li and Y. L. Zhao, *Adv. Mater.*, 2012, **24**, 1226–1231.

132 S. J. Zeng, Z. G. Yi, W. Lu, C. Qian, H. B. Wang, L. Rao, T. M. Zeng, H. R. Liu, H. J. Liu, B. Fei and J. H. Hao, *Adv. Funct. Mater.*, 2014, DOI: 10.1002/adfm.201304270.

133 B. Dong, B. S. Cao, Y. Y. He, Z. Liu, Z. P. Li and Z. Q. Feng, *Adv. Mater.*, 2012, **24**, 1987–1993.

134 B. S. Cao, J. L. Wu, N. S. Yu, Z. Q. Feng and B. Dong, *Thin Solid Films*, 2014, **550**, 495–498.

135 Z. P. Li, B. Dong, Y. Y. He, B. S. Cao and Z. Q. Feng, *J. Lumin.*, 2012, **132**, 1646–1648.

136 X. Bai, H. W. Song, G. H. Pan, Y. Q. Lei, T. Wang, X. G. Ren, S. Z. Lu, B. Dong, Q. L. Dai and L. B. Fan, *J. Phys. Chem. C*, 2007**, 111**, 13611–13617.

137 R. H. Page, K. I. Schaffers, P. A. Waide, J. B. Tassano, S. A. Payne and W. F. Krupke, *J. Opt. Soc. Am. B*, 1998, **15**, 996–1008.

138 J.-C. Boyer and F. C. J. M. van Veggel, *Nanoscale*, 2010, **2**, 1417–1419.

139 J. B. Zhao, Z. D. Lu, Y. D. Yin, C. Mcrae, J. A. Piper, J. M. Dawes, D. Y. Jin and E. M. Goldys, *Nanoscale*, 2013, **5**, 944–952.

140 X. J. Xue, S. Y. Uechi, R. N. Tiwari, Z. C. Duan, M. S. Liao, M. Yoshimura, T. Suzuki and Y. Ohishi, *Opt. Mater. Express*, 2013, **3**, 989–999.

141 W. B. Niu, S. L. Wu and S. F. Zhang, *J. Mater. Chem.*, 2010, **20**, 9113–9117.

142 S. L. Wu, Y. H. Ning, J. Chang and S. F. Zhang, *J. Lumin.*, 2013, **143**, 492–497.

143 N. Bogdan, F. Vetrone, G. A. Ozin and J. A. Capobianco, *Nano Lett.*, 2011, **11**, 835–840.

144 H. Schäfer, P. Ptacek, O. Zerzouf and M. Haase, *Adv. Funct. Mater.*, 2008, **18**, 2913–2918.

145 Y. Wang, L. P. Tu, J. W. Zhao, Y. J. Sun, X. G. Kong and H. Zhang, *J. Phys. Chem. C*, 2009, **113**, 7164–7169.

146 F. Wang, J. Wang and X. G. Liu, *Angew. Chem. Int. Ed.*, 2010, **49**, 7456–7460.

147 W. Zheng, S. Y. Zhou, Z. Chen, P. Hu, Y. S. Liu, D. T. Tum H. M. Zhu, R. F. Li, M. D. Huang and X. Y. Chen, *Angew. Chem. Int. Ed.*, 2013, **52**, 6671–6676.

148 K. A. Abel, J.-C. Boyer and F. C. J. M. van Veggel, *J. Am. Chem. Soc.*, 2009, **131**, 14644–14645.

149 K. A. Abel, J-C Boyer, C. M. Andrei and F. C. J. M. van Veggel, *J. Phys. Chem. Lett.*, 2011, **2**, 185–189.

150 N. J. J. Johnson, A. Korinek, C. H. Dong and F. C. J. M. van Veggel, *J. Am. Chem. Soc.*, 2012, **134**, 11068−11071.

151 F. Zhang, R. C. Che, X. M. Li, C. Yao, J. P. Yang, D. K. Shen, P. Hu, W. Li and D. Y. Zhao, *Nano Lett.*, 2012, **12**, 2852−2858.

152 Y. F. Wang, L. D. Sun, J. W. Xiao, W. Feng, J. C. Zhou, J. Shen and C. H. Yan, *Chem.−Eur. J.*, 2012, **18**, 5558−5564.

153 K. Prorok, A. Bednarkiewicz, B. Cichy, A. Gnach, M. Misiak, M. Sobczyk and W. Strek, *Nanoscale*, 2014, **6**, 1855−1864.

154 F. Vetrone, R. Naccache, V. Mahalingam, C. G. Morgan and J. A. Caopobianco, *Adv. Funct. Mater.*, 2009, **19**, 2924–2929.

155 X. M. Liu, X. G. Kong, Y. L. Zhang, L. P. Tu, Y. Wang, Q. H. Zeng, C. G. Li, Z. Shi and H. Zhang, *Chem. Commun.,* 2011, **47**, 11957–11959.

156 H. S. Qian and Y. Zhang, *Langmuir*, 2008, **24**, 12123–12125.

157 Q. Q. Dou, N. M. Idris and Y. Zhang, *Biomaterials*, 2013, **34**, 1722–1731.

158 Y. H. Zhang, L. X. Zhang, R. R. Deng, J. Tian, Y. Zong, D. Y. Jin and X. G. Liu, *J. Am. Chem. Soc.*, 2014, **136**, 4893–4896.

159 Y. S. Liu, D. T. Tu, H. M. Zhu, R. F. Li, W. Q. Luo and X. Y. Chen, *Adv. Mater.*, 2010, **22**, 3266–3271.

160 Q. Q. Su, S. Y. Han, X. J. Xie, H. M. Zhu, H. Y. Chen, C.-K. Chen, R.-S. Liu, X. Y. Chen, F. Wang and X. G. Liu, *J. Am. Chem. Soc.*, 2012, **134**, 20849–20857.

161 L. Y. Wang, R. X. Yan, Z. Y. Huo, L. Wang, J. H. Zeng, J. Bao, X. Wang, Q. Peng and Y. D. Li, *Angew. Chem. Int. Ed.*, 2005, **44**, 6054–6057.

162 Z. Q. Li, Y. Zhang and S. Jiang, *Adv. Mater.*, 2008, **20**, 4765–4769.

163 L. D. Sun, J. Q. Gu, S. Z. Zhang, Y. W. Zhang and C. H. Yan, *Sci China Ser B-Chem.*, 2009, **52**, 1590–1595.

164 L. Cheng, K. Yang, M. W. Shao, S.-T. Lee and Z. Liu, *J. Phys. Chem. C*, 2011, **115**, 2686–2692.

165 H. H. Gorris, R. Ali, S. M. Saleh and O. S. Wolfbeis, *Adv. Mater.*, 2011, **23**, 1652–1655.

166 R. R. Deng, X. J. Xie, M. Vendrell, Y.-T. Chang and X. G. Liu, *J. Am. Chem. Soc.*, 2011, **133**, 20168−20171.

167 C. H. Liu, Z. Wang, H. X. Jia and Z. P. Li, *Chem. Commun.,* 2011, **47**, 4661–4663.

168 S. J. Wu, N. Duan, X. Y. Ma, Y. Xia, H. X. Wang, Z. P. Wang and Q. Zhang, *Anal. Chem.*, 2012, **84**, 6263−6270.

169 L. Yan, Y.-N. Chang, W. Y. Yin, X. D. Liu, D. B. Xiao, G. M. Xing, L. N. Zhao, Z. J. Gu and Y. L. Zha, *Phys. Chem. Chem. Phys.,* 2014, **16**, 1576−1582.

170 S. Sarkar, B. Meesaragandla, C. Hazra and V. Mahalingam, *Adv. Mater.*, 2013, **25**, 856–860.

171 H. J. Chen, T. Ming, L. Zhao, F. Wang, L. D. Sun, J. F. Wang and C. H. Yan, *Nano Today*, 2010, **5**, 494–505.

172 T. Ming, H. J. Chen, R. B. Jiang, Q. Li and J. F. Wang, *J. Phys. Chem. Lett.*, 2012, **3**, 191−202.

173 W. Feng, L. D. Sun and C. H. Yan, *Chem. Commun.*, 2009, 4393–4395.

174 H. Zhang, Y. J. Li, I. A. Ivanov, Y. Q. Qu, Y. Huang and X. F. Duan, *Angew. Chem. Int. Ed.*, 2010, **49**, 2865–2868.

175 H. Zhang, D. Xu, Y. Huang and X. F. Duan, *Chem. Commun.,* 2011, **47**, 979–981.

176 N. Liu, W. P. Qin, G. S. Qin, T. Jiang and D. Zhao, *Chem. Commun.,* 2011, **47**, 7671–7673.

177 T. Jiang, Y. Liu, S. S. Liu, N. Liu and W. P. Qin, *J. Colloid Interface Sci.*, 2012, **377**, 81–87.

178 A. Priyam, N. M. Idris and Y. Zhang, *J. Mater. Chem.*, 2012, **22**, 960–965.

179 P. Y. Yuan, Y. H. Lee, M. K. Gnanasammandhan, Z. P. Guan, Y. Zhang and Q. H. Xu, *Nanoscale*, 2012, **4**, 5132–5137.

180 M. Saboktakin, X. C. Ye, S. J. Oh, S.-H. Hong, A. T. Fafarman, U. K. Chettiar, N. Engheta, C. B. Murray and C. R. Kagan, *ACS NANO*, 2012, **6**, 8756–8766.

181 M. Saboktakin, X. C. Ye, U. K. Chettiar, N. Engheta, C. B. Murray and C. R. Kagan, *ACS NANO*, 2013, **7**, 7186–7192.

182 S. Schietinger, T. Aichele, H.-Q. Wang, T. Nann and O. Benson, *Nano Lett.*, 2010, **10**, 134–138.

183 H. P. Paudel, L. L. Zhong, K. Bayat, M. F. Baroughi, S. Smith, C. Lin, C. Y. Jiang, M. T. Berry and P. S. May, *J. Phys. Chem. C*, 2011, **115**, 19028–19036.

184 Q. Luu, A. Hor, J. Fisher, R. B. Anderson, S. Liu, T.-S. Luk, H. P. Paudel, M. F. Baroughi, P. S. May and S. Smith, *J. Phys. Chem. C*, 2014, **118**, 3251−3257.

185 Q.-C. Sun, H. Mundoor, J. C. Ribot, V. Singh, I. I. Smalyukh and P. Nagpal, *Nano Lett.*, 2014, **14**, 101–106.

186 Z. Q. Li, L. M. Wang, Z. Y. Wang, X. H. Liu and Y. J. Xiong, *J. Phys. Chem. C*, 2011, **115**, 3291–3296.

187 S. W. Wu, G. Han, D. J. Milliron, S. Aloni, V. Altoe, D. V. Talapin, B. E. Cohen and P. J. Schuck, *Proc. Natl. Acad. Sci. USA*, 2009, **106**, 10917–10921.

188 J. B. Zhao, D. Y. Jin, E. P. Schartner, Y. Q. Lu, Y. J. Liu, A. V. Zvyagin, L. X. Zhang, J. M. Dawes, P. Xi, J. A. Piper, E. M. Goldys and T. M. Monoro, *Nat. Nanotechnol.*, 2013, **8**, 729–734.

189 D. J. Gargas, E. M. Chan, A. D. Ostrowski, Shaul Aloni, M. V. P. Altoe, E. S. Barnard, B. Sanii, J. J. Urban, D. J. Milliron, B. E. Cohen and P. J. Schuck, *Nat. Nanotechnol.*, 2014, **9**, 300–305.

190 Q. Q. Zhan, J. Qian, H. J. Liang, G. Somesfalean, D. Wang, S. He, Z. G. Zhang and S. Andrsson-Engels, *ACS NANO*, 2011, **5**, 3744–3757.

191 G. Y. Chen, T. Y. Ohulchanskyy, A. Kachynski, H. Ågren and P. N. Prasad, *ACS NANO*, 2011, **5**, 4981–4986.

192 W. Q. Zou, C. Visser, J. A. Maduro, M. S. Pshenichnikov and J. C. Hummelen, *Nat. Photonics*, 2012, **6**, 560–564.

193 Y. F. Wang, G. Y. Liu, L. D. Sun, J. W. Xiao, J. C. Zhou and C. H. Yan, *ACS NANO*, 2013, **7**, 7200–7206.

194 J. Shen, G. Y. Chen, A.-M Vu, W. Fan, O. S. Bilsel, C.-C. Chang and G. Han, *Adv. Opt. Mater.*, 2013, **1**, 644–650.

195 X. J. Xie, N. Y. Gao, R. R. Deng, Q. Sun, Q. H. Xu and X. G. Liu, *J. Am. Chem. Soc.*, 2013, **135**, 12608−12611.

196 H. L. Wen, H. Zhu, X. Chen, T. F. Hung, B. L. Wang, G. Y. Zhu, S. F. Yu and F. Wang, *Angew. Chem. Int. Ed.*, 2013, **52**, 13419−13423.

197 Y. T. Zhong, G. Tian, Z. J. Gu, Y. J. Yang, L. Gu, Y. L. Zhao, Y. Ma and J. N. Yao, *Adv. Mater.*, 2014, **26**, 2831−2837.

198 X. M. Li, R. Wang, F. Zhang, L. Zhou, D. K. Shen, C. Yao and D. Y. Zhao, *Sci. Rep.*, 2013, DOI:10.1038/srep03536.

199 M. Wang, C. C. Mi, W. X. Wang, C. H. Liu, Y. F. Wu, Z. R. Xu, C. B. Mao and S. K. Xu, *ACS NANO*, 2009, **3**, 1580−1586.

200 L. C. Ong, L. Y. Ang, S. Alonso and Y. Zhang, *Biomaterials*, 2014, **35**, 2987−2998.

201 S. F. Lim, R. Riehn, W. S. Ryu, N. Khanarian, C.-K. Tung, D. Tank and R. H. Austin, *Nano Lett.*, 2006, **6**, 169−174.

202 J. C. Zhou, Z. L. Yang, W. Dong, R. J. Tang, L. D. Sun and C. H. Yan, *Biomaterials*, 2011, **32**, 9059−9067.

203 Q. Liu, Y. Sun, T. S. Yang, W. Feng, C. G. Li and F. Y. Li, *J. Am. Chem. Soc.*, 2011, **133**, 17122–17125.

204 G. Y Chen, J. Shen, T. Y. Ohulchanskyy, N. J. Patel, A. Kutikov, Z. P. Li, J. Song, R. K. Pandey, H. Ågren, P. N. Prasad and G. Han, *ACS NANO*, 2012, **6**, 8280–8287.

205 T. S. Yang, Y. Sun, Q. Liu, W. Feng, P. Y. Yang and F. Y. Li, *Biomaterials*, 2012, **33**, 3733–3742.

206 Q. F. Xiao, X. P. Zheng, W. B. Wu, W. Q. Ge, S. J. Zhang, F. Chen, H. Y. Xing, Q. G. Ren, W. P. Fan, K. L. Zhao, Y. Q. Hua and J. L. Shi, *J. Am. Chem. Soc.*, 2013, **135**, 13041–13048.

207 Y. Sun, X. J. Zhu, J. J. Peng and F. Y. Li, *ACS NANO*, 2013, **7**, 11290–11300.

208 D. L. Ni, J. W. Zhang, W. B. Wu, H. Y. Xing, F. Han, Q. F. Xiao, Z. W. Yao, F. Chen, Q. J. He, J. N. Liu, S. J. Zhang, W. P. Fan, L. P. Zhou, W. J. Peng and J. L. Shi, *ACS NANO*, 2014, **8**, 1231–1242.

209 P. A. Ma, H. H. Xiao, X. X. Li, C. X. Li, Y. L. Dai, Z. Y. Cheng, X. B. Jing and J. Lin, *Adv. Mater.*, 2013, **25**, 4898–4905.

210 Y. L. Dai, H. H. Xiao, J. H. Liu, Q. H. Yuan, P. A. Ma, D. M. Yang, C. X. Li, Z. Y. Cheng, Z. Y. Hou, P. P.Yang and J. Lin, *J. Am. Chem. Soc.*, 2013, **135**, 18920–18929.

211 G. Han, T. Mokari, C. Ajo-Franklin and B. E. Cohen, *J. Am. Chem. Soc.*, 2008, **130**, 15811–15813.

212 Y. Zou, T. Yi, S. Z. Xiao, F. Y. Li, C. Y. Li, X. Gao, J. C. Wu, M. X. Yu and C. H. Huang, *J. Am. Chem. Soc.*, 2008, **130**, 15750–15751.

213 R. Klajn, P. J. Wesson, K. J. M. Bishop and B. A. Grzybowski, *Angew. Chem. Int. Ed.*, 2009, **48**, 7035–7039.

214 C. Zhang, H. P. Zhou, L. Y. Liao, W. Feng, W. Sun, Z. X. Li, C. H. Xu, C. J. Fang, L. D. Sun, Y. W. Zhang and C. H. Yan, *Adv. Mater.* 2010, **22**, 633–637.

215 C.-J. Carling, J.-C. Boyer and N. R. Branda, *J. Am. Chem. Soc.*, 2009, **131**, 10838–10839.

216 C.-J. Carling, F. Nourmohammadian, J.-C. Boyer and N. R. Branda, *Angew. Chem. Int. Ed.*, 2010, **49**, 3782–3785.

217 M. K. G. Jayakumar, N. M. Idris and Y. Zhang, *Proc. Natl. Acad. Sci. USA*, 2012, **109**, 8483–8488.

218 W. Wu, L. M. Yao, T. S. Yang, R. Y. Yin, F. Y. Li and Y. L. Yu, *J. Am. Chem. Soc.*, 2011, **133**, 15810–15813.

219 L. Wang, H. Dong, Y. N. Li, X. M. Chen, L. D. Sun, C. H. Yan and Q. Li, *J. Am. Chem. Soc.*, 2014, **136**, 4480−4483.

220 X. F. Qiao, J. C. Zhou, J. W. Xiao, Y. F. Wang, L. D. Sun and C. H. Yan, *Nanoscale*, 2012, **4**, 4611–4623.

221 N. M. Idris, M. K. Gnanasammandhan, J. Zhang, P. C. Ho, R. Mahendran and Y. Zhang, *Nat. Med.*, 2012, **18**, 1580–1586.

222 H. P. Zhou, C. H. Xu, W. Sun and C. H. Yan, *Adv. Funct. Mater.*, 2009, **19**, 3892–3900.

223 Y. Liu, M. Chen, T. Y. Cao, Y. Sun, C. Y. Li, Q. Liu, T. S. Yang, L. M. Yao, W. Feng and F. Y. Li, *J. Am. Chem. Soc.*, 2013, **135**, 9869−9876.

224 D. J. Naczynski, M. C. Tan, M. Zevon, B. Wall, J. Kohl, A. Kulesa, S. Chen, C. M. Roth, R. E. Riman and P. V. Moghe, *Nat. Commun.*, 2013, DOI:10.1038/ncomms3199.